Stony Brook University

Role of Speciation in Tungstate Sorption on Iron Oxyhydroxides: A Spectroscopic Study

A Thesis Presented

by

Emily Ann Lorenz

to

The Graduate School

in Partial Fulfillment of the

Requirements

for the Degree of

Master of Science

in

Geosciences

Stony Brook University

August 2009

Stony Brook University

The Graduate School

Emily Ann Lorenz

We, the thesis committee for the above candidate for the

Master of Science degree, hereby recommend

acceptance of this thesis.

Richard J. Reeder – Thesis Advisor
Professor, Department of Geosciences

Brian L. Phillips – Chairperson of Defense
Associate Professor, Department of Geosciences

Scott M. McLennan
Professor, Department of Geosciences

This thesis is accepted by the Graduate School

Lawrence Martin
Dean of the Graduate School

Abstract of the Thesis

Role of Speciation in Tungstate Sorption on Iron Oxyhydroxides: A Spectroscopic Study

by

Emily Ann Lorenz

Master of Science

in

Geosciences

Stony Brook University

2009

Tungsten is a largely unregulated transition metal that is used in many industrial, military and civil applications despite the fact that ity in the environment and toxicity are not fully understood. In this study, we investigate the effect of speciation on tungstate sorption, which is one of the dominant mechanisms controlling metal mobil These experiments combine speciation calculations, X-ray absorption spectroscopy (XAS) and differential pair distribution function (PDF) data to describe adsorption at the goethite and ferrihydrite surfaces over a range of pH and concentration conditions. W L_{III}-edge EXAFS and W L_I-edge XANES of tungstate solutions show at least one polymeric species present in solution at pH 4 and orthotungstate species dominant at pH 8, which is consistent with speciation calculations. XAS data of sorption samples prepared using different sorbents (goethite, ferrihydrite) over a range of pH (4-8) and tungsten concentration (25-1000 μM) show spectra that are similar. The results suggest

that tungstate polymerizes at the surface of these iron oxides, forming a polytungstate sorption complex, or possibly a surface precipitate. This conclusion is supported by the differential PDF data, which show correlations extending to 11 Å that are likely attributable to the W-W pair correlations present in polytungstates. Our findings provide information pertaining to the environmental fate of tungsten and stress the need for additional research to properly assess its regulatory status

I would like to thank my family for everything.

Table of Contents

List of Figures……....vii

List of Tables……..ix

Acknowledgements……..x

1. Introduction……..1

2. Materials and Methods…….....5

2.1. Materials and Reagents…….5

2.2 Model Compounds…….5

2.3. Goethite Synthesis……6

2.4. Batch Sorption Experiments…….7

2.5. Solution analysis……..……8

2.6. X-ray Absorption Spectroscopy (XAS)……9

3. Results……11

3.1. Aqueous Speciation……11

3.2. Batch Uptake Experiments……19

3.3. XANES Data……..…21

3.4. EXAFS results for solution samples at pH 4, 6 and 8…...……26

3.5. EXAFS results for model compounds……31

3.6. EXAFS analysis of sorption samples……..……34

3.7. Differential PDF data of Ferriydrite Sorption Samples……..……40

4. Discussion……..43

5. Conclusions and Implications……47

References……..48

List of Figures

Figure 1. Polyhedral representations of (a) orthotungstate (WO_4^{-2}), (b) paratungstate A ($W_7O_{24}^{-6}$), (c) paratungstate B ($H_2W_{12}O_{42}^{-10}$) and (d) α– metatungstate ($H_2W_{12}O_{40}^{-6}$)……....13

Figure 2. Aqueous tungstate polymerization at various pH conditions (modified from Smith and Patrick, 2000; van Put, 1995)……...16

Figure 3. Calculated W(VI) speciation at a) 0.1 M, b) 0.0027 M and c) 0.00005 M.…...18

Figure 4. Adsorption isotherm of tungsten on goethite from a solution at pH 4.0, with 0.3 g/L Fe as goethite, and background electrolyte 0.01 M NaCl.….……....19

Figure 5. pH dependence of W sorption on goethite. Total W = 50 μM, 0.3 g/L Fe (as FeOOH), and background electrolyte is 0.01 M NaCl.……..…20

Figure 6a-d. Normalized W L_I-edge XANES spectra…….....23

Figure 7. Normalized W L_I-edge XANES spectra for 2.7 mM W solutions at pH 4, 6 and 8 (dotted lines) as well as model compounds $Na_2WO_4 \cdot H_2O$, $H_3PO_4 \cdot 12WO_3 \cdot xH_2O$ and Ba_2NiWO_6 (solid lines) for comparison……..……...24

Figure 8. Normalized W L_I-edge XANES spectra for 50 μM W sorbed on goethite, pH 4 (dotted line) as well as model compounds $Na_2WO_4 \cdot H_2O$, $H_3PO_4 \cdot 12WO_3 \cdot xH_2O$ and Ba_2NiWO_6 (solid lines) for comparison……25

Figure 9. (a) k^3-weighted W L_{III}-edge EXAFS data of the 2.7 mM solution at pH 8, and (b) corresponding Fourier transforms…….….....26

Figure 10. (a) k^3-weighted W L_{III}-edge EXAFS data of the 2.7 mM solution at pH 4, and (b) corresponding Fourier transforms in raw (dotted lines) and fitted data (solid lines)……28

Figure 11. (a) W L_{III}-edge k^3-weighted EXAFS data of 2.7 mM W solution at pH 4, 6 and 8 (dotted lines) with k^3-weighted linear combination fit of the pH 6 solution (solid line) and (b) the Fourier transform of solution at pH 6……..……30

Figure 12. (a) W L_{III}-edge k^3-weighted EXAFS data of model compounds (H_2WO_4, WO_3, ferberite, scheelite, Na_2WO_4) and (b) the corresponding Fourier transforms (not corrected for phase shift)……..32

Figure 13. (a) k^3-weighted W L_{III}-edge EXAFS data for Na_2WO_4, WO_3, ferberite and tungsten sorption samples of various concentrations at pH 4, 6 and 8, and (b) corresponding Fourier transforms……..……..…….35

Figure 14. (a) k^3 –weighted W L_{III}-edge EXAFS data of 50 μM W sorbed at the surface of 0.5 g/L goethite at pH 4 with varied k ranges and (b) corresponding Fourier transforms……..... 37

Figure 15. (a) fit of k^3-weighted W L_{III}-edge EXAFS data of the 50 μM W on 0.5 g/L goethite at pH 4 without W-Fe paths (above) and with W-Fe paths (below), and (b) corresponding Fourier transforms……...38

Figure 16. (a) k^3-weighted W L_{III}-edge EXAFS data of the 50 μM W on 0.477 g/L goethite at pH 4 (solid line) and 5 mM W on 0.5 g/L ferrihydrite at pH 4 (dotted line), and (b) corresponding Fourier transforms……...……41

Figure 17. Differential PDF spectrum of 5 mM tungsten sorbed on 2-line ferrihydrite at pH 4……....42

List of Tables

Table 1. Approximated equilibrium constants (Smith and Patrick, 2000)……12

Table 2. Average interatomic distances for several polytungstates including the octahedral oxygens and average W-W distances for each structure….....14

Table 3. W L_{III}-edge EXAFS fitting results of 2.7 mM solution at pH 8..……...27

Table 4. W L_{III}-edge EXAFS fitting results of 2.7 mM solution at pH 4 using (a) single scatter paths only, and (b) both single and W-O multiple scatter paths……29

Table 5. W L_{III}-edge EXAFS fitting results of model compounds……33

Table 6. W L_{III}-edge EXAFS fit results of 50 μM W sorbed on 0.5 g/L goethite at pH 4 using (a) without W-Fe paths and (b) with W-Fe paths……..…….3

Acknowledgements

I would like to express my sincere thanks to my advisor, Dr. Richard J. Reeder, for all of his guidance during my time at Stony Brook University.

1. Introduction

Speciation, which describes the oxidation state, coordination, stoichiometry and physical state of an element, is critical in understan l behavior. Speciation controls solubility and uptake behaviors, which in turn influence mobility. Understanding the mobility of an element in the environment is necessary in an assessment of its bioavailability. Significant factors affecting mobility include dissolution/precipitation, reduction/oxidation and sorption/desorption reactions (Reeder et al. 2006). A clear understanding of these mechanisms is essential in an evaluation of the long-term environmental and health effects associated with an element.

Tungsten is a transition metal typically found as a trace element in soils, though higher tungsten concentrations are present in certain areas due to mineral-rich deposits or anthropogenic activity (Koutsospyros et al. 2006; Strigul et al. 2009). The average concentration of tungsten in Earth's crust is 1.55 ppm (Koutsospyros et al., 2006). Typical concentrations of tungsten in surface rocks are 1.0-1.3 ppm and in surface soils are 0.68-2.7 ppm (Koutsospyros et al., 2006). Tungsten occurs in a variety of oxidation states ranging from -2 to +6 (Koutsospyros et al., 2006); the form that is stable in the environment is +6 (ATSDR, 2005). Naturally, tungsten occurs in more than twenty minerals, the most common of which are scheelite ($CaWO_4$) and wolframite (a solid solution with ferberite ($FeWO_4$) and huebnerite ($MnWO_4$) as end members) (ATSDR, 2005). While tungsten does not occur as pure metal naturally, it is mined to produce pure metal and alloys that are used in industrial (e.g., hardmetal), civil (e.g., light bulb filaments) and military (e.g., ammunition) applications (Seiler et al., 2005; Koutsospyros et al., 2006; Bednar et al., 2008). With all of these uses and the lack of knowledge

regarding tungsten mobility in the environment and its toxicity, it is surprising that, with the exception of an occupational exposure limit, tungsten is completely unregulated in the United States and Western Europe (Petkewich, 2009; Str gul et al., 2009). The lack of drinking water and discharge standards is likely due to the fact that, until recently, tungsten was thought to be insoluble in water and non-toxic. In fact, it is for these reasons that in the mid-1990's, the United States Army replaced lead in bullets with tungsten alloys (Petkewich, 2009).

It is now known that tungsten is soluble under certain environmental conditions, allowing it to readily move through soils and into groundwater. Studies have shown that in addition to tungstate minerals, anthropogenic tungsten powders are soluble. For example, in a study of three firing ranges at Camp Edwards in the Massachusetts Military Reservation, tungsten concentrations in the groundwater were found to be 0.001-4 ppm, which is above the background concentration of tungsten in the area, which is less than 0.0002 ppm (Clausen, J. L. and Korte, N., 2009). Dissolution of tungsten containing powders have been shown to decrease solution pH (Dermatas, 2004), which affects speciation. A clear understanding of speciation and its effect on sorption is critical for a full assessment of tungsten toxicity and mobility. Th is made difficult by inconsistencies in the available thermodynamic data for aqueous tungstate species, which will be discussed later in this work. In short, upon acidification, tungstate (WO_4^{-2}), which is the dominant form at high pH, polymerizes forming a number of soluble polytungstates (Kepert, 1969). A complete understanding of the tungstate system is made difficult by the existence of numerous species and the slow kinetics of polymerization, which may

take up to eight months to reach equilibrium (Smith and Patrick, 2000). The realization that tungsten is in fact soluble raises questions pertaining to its toxicity.

The need for greater scrutiny regarding the health effects associated with tungsten was highlighted by several reports of elevated levels of tungsten in the tap water (0.25-337 ppm W) and urine (as much as 15 times more than the national average) of the residents of Fallon, Nevada., which was in turn proposed as a possible cause for a childhood leukemia cluster affecting the population (e.g. Koutsospyros et al., 2006). Sixteen reported leukemia cases in Fallon in 1997-2001 raised enough concern that the Centers for Disease Control (CDC) and the National Center for Environmental Health (NCEH) ordered toxicological and carcinogenic studies (Koutsospyros et al., 2006). In addition, the Environmental Protection Agency (EPA) has included tungsten compounds on its Priority Testing List, and in 2008 tungsten was acknowledged as an emerging pollutant (Strigul et al., 2009). Studies now suggest that the cancer cluster at Fallon may have more to do with genetic than environmental factors, but this topic is still being debated. Preliminary toxicity reports provide little evidence that tungsten may pose a serious threat to human health (Pardus et al., 2009). New studies, however, suggest that for a variety of organisms, sodium metatungstate (a polytungstate) is significantly more toxic than sodium tungstate (a monotungstate) (Strigul et al. a, in press; Strigul et al. b, in press). Since most toxicological studies have used sodium monotungstate or metallic tungsten (Pardus, 2009), additional research addressing the effects of speciation on toxicity is necessary. The need for this research is made more urgent by the fact that tungsten is now known to be soluble under certain conditions causing a decrease in pH, which could facilitate polytungstate formation in the environment.

Tungsten and molybdenum exhibit similarities in chemical behavior inasmuch as they occur in the same group in the periodic table (Xu, 2006), though generally isopolytungstates adopt structures different from isopolymolybdates (Pope, 1983). It is known that tungstate can render certain molybdate-based enzymes inactive by replacing the molybdate (Johnson et al., 1974; Johnson and Rajagopolan, 1976; Bednar, 2008), which would contribute to tungsten toxicity. Nevertheless, some similarities in sorption behavior may exist. Tungsten has been shown to sorb competitively with molybdate at the goethite (FeOOH) and ferrihydrite surface (Xu, 2006; Xu, 2009; Gustafsson, 2003).

The focus of this study is to investigate the environmental fate of tungsten, which has become the focus of many recent studies. It has been shown that tungstate sorbs strongly to the goethite surface over a range of pH and is irreversibly sorbed at pH < 5, which may prove effective if remediation is ever necessary (Xu et al., 2006; Xu et al., 2009). The charge distribution multi-site complexation (CD-MUSIC) model has predicted that tungstate sorbs to goethite as a monodentate mononuclear complex (Xu et al., 2009; Xu et al., 2006), though no known direct spectroscopic evidence exists to support this. There has been no known study addressing the effect of speciation on tungstate adsorption. Since speciation controls behavior, influencing mobility and toxicicty, understanding its effect on sorption is essential. Since sorption products may behave differently, understanding the type of complex and the mode of sorption is necessary to understand tungsten's environmental behavior. The purpose of this study has been to examine the effect of speciation on tungstate sorption at the goethite and ferrihydrite mineral surfaces over a range of environmentally relevant pH and concentration conditions. Goethite and ferrihydrite are chosen because of their

widespread occurrence in soils and their capacity to sorb heavy metals. This work is achieved by combining batch uptake experiments and spectroscopic analyses at the W L_I and L_{III}-edges. XAS is a useful tool for investigating sorption modes of metals because it is element specific and can provide direct information regarding the local coordination of an atom to ~5 Å. W L_{III}-edge EXAFS is useful as it provides information regarding the local environment of tungsten including the number of nearest neighbors and their distances. W L_I- edge XANES is useful because of its sensitivity for distinguishing coordination geometry. This study concludes that tungstate sorbs to goethite and ferrihydrite over a wide range of pH and concentration conditions as polytungstate species, even when orthotungstate is dominant in solution.

2. Materials and Methods

2.1. Materials and reagents

All sorption experiments were performed under atmospheric conditions. All chemicals were obtained from Alfa Aesar with the exception of phosphotungstic acid ($H_3PO_4 \cdot 12WO_3 \cdot xH_2O$), which was obtained from Sigma Aldrich. Tungsten stock solutions were prepared using Na_2WO_4?$2H_2O$ and deionized water. Tungsten was added to suspensions using 0.01 M or 1.0 M stock solutions, which were freshly prepared for each set of experiments to avoid precipitates.

2.2. Model Compounds

Eight model compounds were used for XAS analysis and interpretation. Tetrahedrally coordinated tungsten model compounds include the mineral scheelite

($CaWO_4$) and $Na_2WO_4 \cdot 2H_2O$ as well as anhydrous sodium tungstate (Na_2WO_4). Octahedrally-coordinated tungsten model compounds include phosphotungstic acid ($H_3PO_4 \cdot 12WO_3 \cdot xH_2O$), which has distorted edge and corner-sharing octahedra, the mineral ferberite ($FeWO_4$), which has distorted edge-sharing octahedra, tungstic acid monohydrate (H_2WO_4) and tungsten trioxide (WO_3), which both have distorted corner-sharing octahedra and Ba_2NiWO_6, which has perfect octahedral symmetry.

Drying of $Na_2WO_4 \cdot 2H_2O$ at 400 °C for one week resulted in anhydrous sodium tungstate, which was transported to the beamline for data collection within three hours to prevent rehydration. Ba_2NiWO_6 was synthesized by mixing and grinding $BaCO_3$ (Alfa Aesar), $NiCO_3$ (Alfa Aesar) and WO_3 (Alfa Aesar). The mixture was then heated at 1100 °C for 20 hours, reground and heated at 1150 °C for 12 hours (Yamazoe, 2008). All identities were confirmed using X-ray diffraction.

2.3. Goethite Synthesis

Goethite was synthesized as described by Schwertmann and Cornell (1991). Necessary concentrations of $Fe(NO_3)$ and KOH were reacted at 70 °C for 60 hours followed by centrifugation, rinsing and drying. The synthesized material was characterized using x-ray diffraction, which shows goethite as the only phase. SEM imaging shows the elongated acicular crystalline structure typical of this mode of synthesis. The surface area of 52 m^2/g was determined for the synthesized goethite using a multipoint BET isotherm with N_2 as the adsorbate. An additional sorption sample of tungsten on ferrihydrite was used for comparison with the goethite samples. The 2-line

ferrihydrite was synthesized by Douglas B. Hausner (of Temple University) using Schwertmann and Cornell's method (1991).

2.4. Batch Sorption Experiments

All experiments were performed at room temperature under atmospheric conditions. No attempt was made to exclude CO_2 because FTIR data, which we collected, indicates that tungstate competitively sorbs replacing any carbonate at the goethite surface at pH 4, 6 and 8. A 0.01 M NaCl solution was prepared using deionized water, and 0.477 g /L goethite (0.3 g/L Fe as goethite) was added. For the ferrihydrite experiments, a 0.01 M $NaNO_3$ solution was prepared and 0.5 g/L ferrihydrite was added. Total volumes of all suspensions were 250 mL. NaCl and $NaNO_3$ were chosen as background electrolytes because they were used successfully in previous studies for similar experiments (Xu et al., 2006; Gustafsson, 2003 found no evidence of precipitation in any of our experiments to suggest reaction with the background electrolyte. The suspensions equilibrated overnight before being titrated to desired pH values using HCl or HNO_3 and NaOH. After an additional 24 h equilibration time, desired tungsten concentrations were added from a stock solution while pH was monitored and adjusted as necessary. The pH of a 0.01 M W stock solution is ~7.2. Sorption experiments reacted for 24 h before filtration using a vacuum pump. Wet pastes were collected for XAS analysis. Certain sorption samples were dried in the oven at 60 C for XAS analysis. Solutions from the goethite sorption experiments were kept for DCP analysis. Surface coverage was calculated to determine an appropriate range of adsorbate concentrations for our experiments, so as to ensure that the surface was not overloaded

with tungsten, which may favor surface precipitation. The concentration of sorbing surface sites was calculated using

$$\text{sorbing surface sites (mol sites/L)} = \frac{N_S\ (\text{sites/m}^2) \times S_A\ (\text{m}^2/\text{g}) \times C_S\ (\text{g/L})}{N_A\ (\text{sites/mol sites})},$$

where N_S is the surface site density, S_A is the surface area, C_S is the weight of sorbent in contact with a liter of solution and N_A is Avogadro's number (Langmuir, 1997). From these calculations, using the published range for surface site density (2.6-16.8 sites/nm^2) (Davis and Kent, 1990) and assuming 100% sorption, 50 μmol/L tungsten was found to cover approximately 7-45 % of the goethite surface, which is a desirable range for XAS. In addition, one lower (25 μmol/L) and multiple higher (100-1000 μmol/L) concentrations of tungsten were used for experiments to determine the effect on adsorption.

2.5. Solution analysis

A 20 mL aliquot of solution from each sorption experiment was collected and filtered through 0.45 μm pore size filter. 20 μL of NaOH was added to prevent precipitate formation. Solutions were analyzed for total W concentration using a direct current argon plasma emission spectrophotometer (DCP-AES). The detection limit for tungsten corresponding to the wavelength used for analysis is 0.02 mg/L. For every two samples analyzed, a two-point calibration curve was calculated. To determine the best technique for consistent recovery, known tungsten concentrations were added to 0.01 M NaCl solutions in glass, polyethylene and teflon bottles, in triplicate. To one, 20 μL

HNO_3 was added; to another 20 µL NaOH was added. Nothing was added to the third (blank). DCP analyses of the acidified solutions yielded results depleted in W, which we interpreted as indicating precipitation. The basic and blank solutions gave results in which total W was conserved. NaOH was chosen, because experiments were performed over a wide range of pH. Other experimenters have added hydrogen peroxide to solutions to ensure recovery; we compared the H_2O_2 method with the procedure we developed and found the results consistent. The container type had no discernable effect, so polyethylene Nalgene bottles were used. Tungsten (1000 mg/L) in H_2O AAS standard was purchased (SPEX CertiPrep), and diluted using 0.01 l solutions to create working standards. The pH of the purchased standard is approximately 10.5, causing each prepared standard to be basic (pH 8-10). For consistency and to avoid any precipitation, rinsing of the DCP tubing was done between each sample using deionized water titrated to pH ~ 9. The amount of tungsten uptake by the goethite was calculated by subtracting the final solution concentration from the initial solution concentration. Measurements were repeated a minimum of three times and averaged. Precision of the average was determined by the standard error of the replicate measurements.

2.6. X-ray Absorption Spectroscopy (XAS)

Extended X-ray absorption fine structure (EXAFS) spectroscopy data and extended X-ray near edge structure (XANES) spectroscopy data were collected at beamline 20BM at the Advanced Photon Source (Argonne National Laboratory, Argonne, Il.) and at X18B, X11A and X11B at the National Synchrotron Light Source (Brookhaven National Laboratory, Upton, NY.)

EXAFS and XANES data for the model compounds were collected in transmission mode using gas-filled ion chambers. Pre-determined amounts of ferberite, tungstic acid monohydrate, scheelite and Na_2WO_4 were each mixed with boron nitride before loading in aluminum sample holders with two layers of Kapton tape. Na_2WO_4?$2H_2O$, Ba_2NiWO_6, phosphotungstic acid and tungsten trioxide were ground and brushed onto Kapton tape generating a very thin layer of material; the tape folded to obtain an edge jump of 0.8-1.5. Data for sorption and solution samples were collected in fluorescence mode. Each sample was doubly sealed in Lucite holders with Kapton tape to prevent drying and placed at a 45° angle to the incident beam. All fluorescence data were collected using a 13-element Ge detector, with the exception of the ferrihydrite sorption sample for which fluorescence data were collected using a PIPS detector. At X18B, X11A and X11B, a Si(111) channel cut monochromat M, a pair of Si(111) crystals was used. The monochromator was detuned 15% at the W L_{III}-edge and 10% at the W L_I-edge for harmonic rejection. For EXAFS at the W L_{III}-edge (10207 eV), the monochromator was calibrated with either a gallium filter (10367 eV) or a zinc metal foil (9660 eV). For XANES collection at the W L_I-edge (12100 eV), the monochromator was calibrated using a platinum metal foil (11 3 eV). Calibration of the monochromator was achieved by assigning the first peak of the derivative the edge energy of the element used for calibration. The W L_{III}-edge was examined for its usefulness in an investigation of the local environment of tungsten, including the number of nearest neighbors and their distance. The W L_I-edge was examined, because the XANES data collected at this energy are more sensitive to distinguishing certain aspects of coordination.

Data processing was done using WinXAS (Ressler, 1997) T (Newville, 2001). Background subtraction and normalization were performed using a linear pre-edge function and a second order post-edge polynomial. The ?(k) function was extracted using a cubic spline and Fourier transformed using k^3 weighting. Theoretical phases and backscattering amplitudes were calculated using FEFF7 (Zabinsky et al., 1995). Fitting was done in R-space. The amplitude reduction factor (S_0^2) was determined from fitting the model compounds and was fixed at 0.9. value is similar to the range used by other experimenters for tungsten (Hoffman et al., 2000). A global threshold energy value (E_0) was allowed to vary. Errors of fit parameters were estimated on the basis of fits to reference compounds and were found to be ± 20 % for first-shell coordination number and ± 40 % for higher coordination shells, ± 0.02 Å for first-shell distance and ± 0.05 Å for longer distances, and ± 0.0 $Å^2$ for first shell Debye-Waller type factors and ± 0.008 $Å^2$ for longer shells.

3. Results

3.1. Aqueous Speciation

Aqueous tungstate speciation was calculated using the program PHREEQC (Parkhurst and Appelo, 1999) and the LLNL database distributed with the program. Relevant stability constants were added to the input file to calculate speciation. While it has been studied extensively, tungsten speciation is not completely understood due to the existence of multiple polymeric species and the sluggish kinetics involved in their

formation (Kepert, 1969; Pope,1983; Smith and Patrick, 2000). Discrepancies present in the data may be due to use of indirect methods of meas uch as potentiometry, or to an underestimation of the equilibration time, which may be as long as eight months (Smith and Patrick, 2000). As a result of inconsistencies in stability constants, only polytungstate species that have been directly observed in solution using ^{183}W NMR have been included in our calculations. Table 1 provides approximate stability constants for these species: paratungstate A ($W_7O_{24}^{-6}$), paratungstate B ($H_2W_{12}O_{42}^{-10}$) and metatungstate ($H_2W_{12}O_{40}^{-6}$). The constants are considered approximate because variable range of ionic strength due to variable concentrations of highly charged anions present in the experiments make the system non-ideal, and determination of equilibrium constants from non-ideal systems hinders accuracy (Smith and Patrick, 2000). However, these constants are reasonably consistent with those reported by experimenters using lower concentrations (Cruywagen and Merwe, 1987) .

Table 1. Approximated equilibrium constants (at 293 K) (Smith and Patrick, 2000).

Solution Species Reaction	Stability Constant (log K)
$7\ WO_4^{-2} + 8\ H^+ \leftrightarrow W_7O_{24}^{-6} + 4\ H_2O$	68.17
$12\ WO_4^{-2} + 14\ H^+ \leftrightarrow H_2W_{12}O_{42}^{-10} + 6\ H_2O$	118.00
$12\ WO_4^{-2} + 18\ H^+ \leftrightarrow H_2W_{12}O_{40}^{-6} + 8\ H_2O$	144.72

Orthotungstate as well as three polytungstate structures are shown in Figure 1 and accompanied by a list of relevant interatomic distances for each structure (Table 2). For the polytungstate species, edge-shared octahedra place W atoms approximately3.2 to 3.5 Å apart and corner-shared octahedra place W atoms approximately 3.6 to 3.7 Å apart.

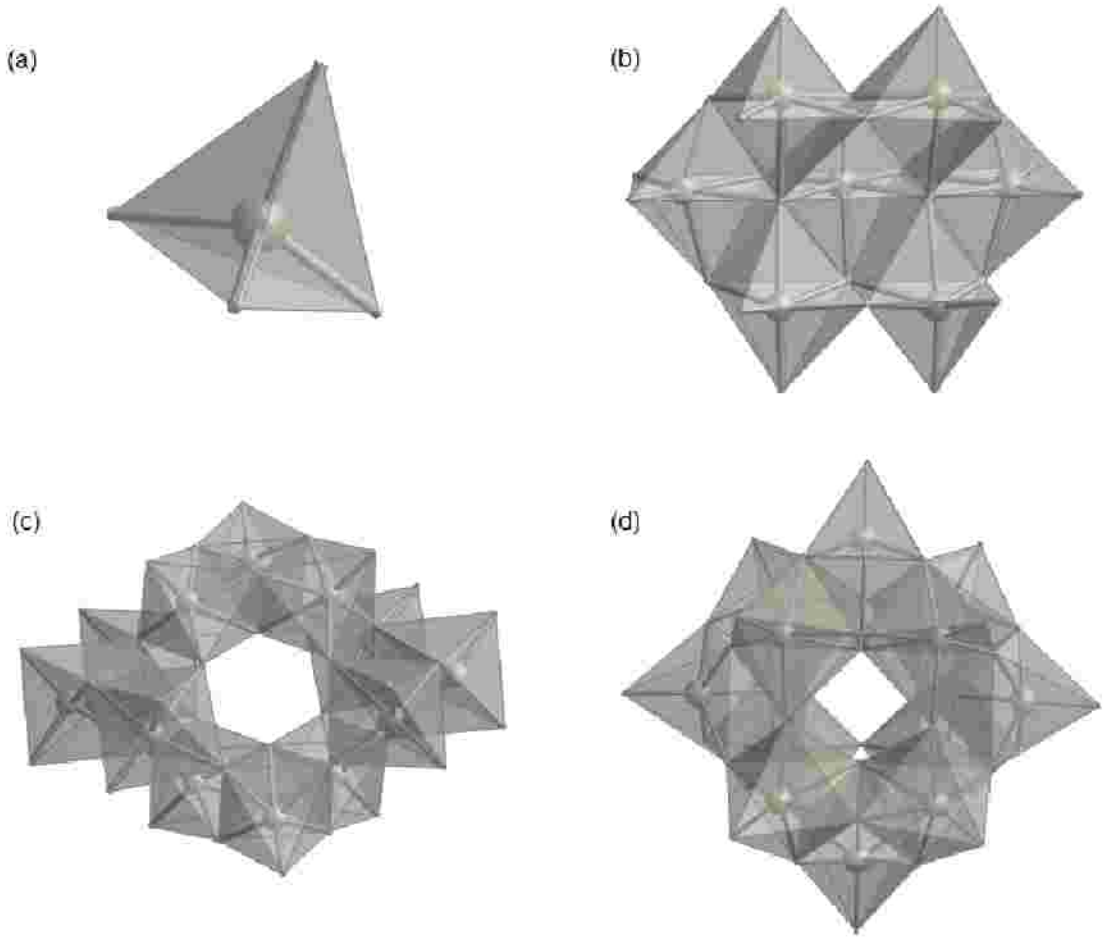

Figure 1. Polyhedral representations of (a) orthotungstate (WO_4^{-2}), (b) paratungstate A ($W_7O_{24}^{-6}$), (c) paratungstate B ($H_2W_{12}O_{42}^{-10}$) and (d) α– metatungstate ($H_2W_{12}O_{40}^{-6}$)

Table 2. Average interatomic distances for several polytungstates including the octahedral oxygens and average W-W distances for each structure.

Species	W-O distances in octahedron (Å)	W-W distances (Å)	Reference
Paratungstate A	1.74 1.81 1.95 2.03 2.23 2.29	3.31 3.48 4.33	Burtseva, K.G., 1978
Paratungstate B	1.73 1.79 1.88 1.94 2.13 2.26	3.31 3.69 4.58	Evans, H.T.jr.; Rollins, O.W, 1976
a-metatungstate (Keggin structure)	1.849 1.879 1.879 2.035 2.035 2.331	3.42 3.63 4.99	Keggin, 1934

An overview of tungstate speciation, including its pH dependence and the influence of kinetics, is presented in Figure 2 (adapted from Smith and Patrick, 2000; van Put, 1995; Pope, 1983; Hastings and Howarth, 1992). Most authors agree that as orthotungstate (WO_4^{-2}) is acidified, paratungstate A ($W_7O_{24}^{-6}$) forms rapidly and then is converted to paratungstate B ($H_2W_{12}O_{42}^{-10}$) over a reported duration of hours to months (Pope, 1983; Smith and Patrick, 2000; van Put, 1995). The dominance of orthotungstate in solution is pH and concentration dependent. At low concentration (50 μM W), it is the dominant species at pH = 5.5. As concentration of tungsten is increased, so is the pH at which orthotungstate is the dominant species. Upon further acidification, a – metatungstate ($H_2W_{12}O_{40}^{-6}$) will form. A number of intermediate species have been reported; however, they are thought to be metastable, short-lived species that are insignificant at equilibrium (van Put, 1995; Smith and Patrick, 2000). These species have not been included in our calculations, because structures and stability constants are not well-defined. It is important to note that our solution XAS experiments were performed within four days of the sorption experiments (not after the estimated eight month equilibration time), so it is possible that some intermediate species are present in our samples.

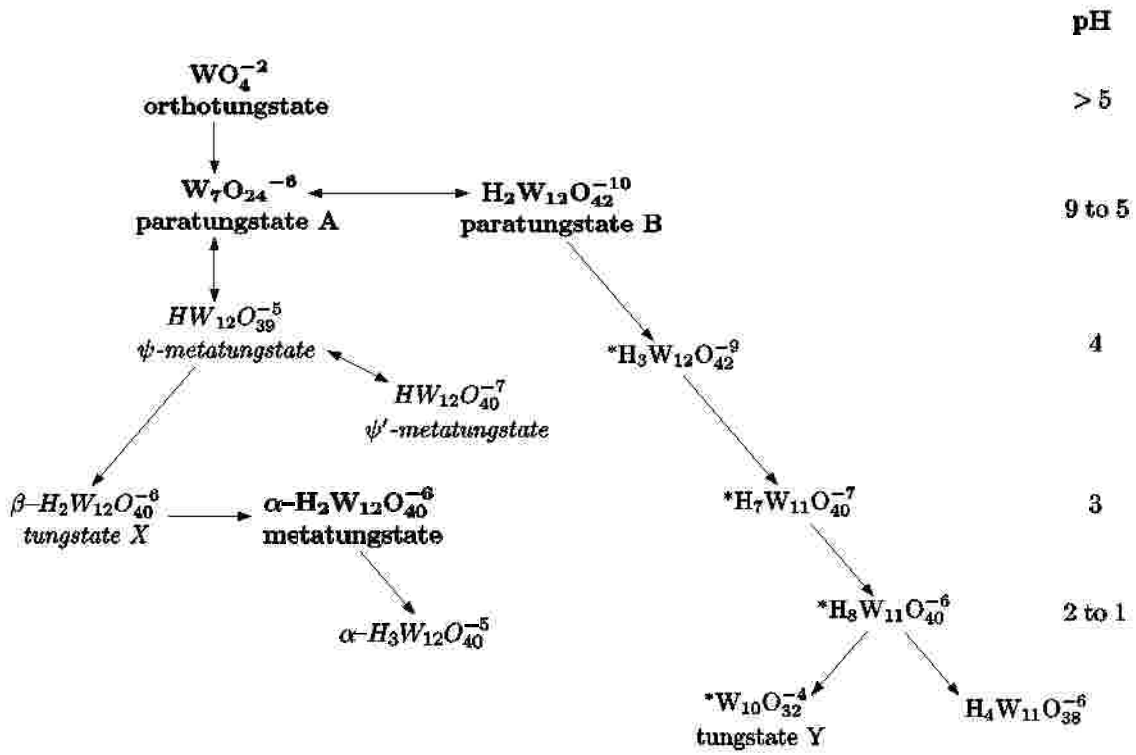

Figure 2. Aqueous tungstate polymerization at various pH conditions. **Bold-typed** species are major stable species; *Italicized* species are those which are intermediate due to thermodynamic instability. (modified from Smith and Patrick, 2000; van Put, 1995). * denotes species that are diff lt to investigate in solution due to low solubilities involved in reaction (Hastings and Howarth, 1992).

In an equilibrated solution with 50 µM W (Fig 3a), a-metatungstate ($H_2W_{12}O_{40}^{-6}$) is the dominant species in the acidic range up to pH = 4.7. Most of the tungsten is present as orthotungstate (WO_4^{-2}) at pH = 4.7. At pH 5.0, paratungstate A ($W_7O_{24}^{-6}$) accounts for 3.6 % of the species present in solution, but this accounts for 7 % of the total tungsten present in solution, because the paratungstate A ion is a heptatungstate. At a tungsten concentration of 2.7 mM W (Fig. 3b), a-metatungstate is dominant up to approximately 5.5. Paratungstate A is the dominant species in solution to pH ~5.8; while it represents

41% of the species present, this is actually 70% of the tungsten present in solution. At pH > 5.8, orthotungstate is the dominant form of tungsten. At pH 6, approximately 16% of tungsten is present as paratungstate B ($H_2W_{12}O_{42}^{-10}$), though this only accounts for 6% of the species in solution since each ion contains 12 tungsten atoms. As the tungsten concentration in an equilibrated solution increases to 0.1 M W(Fig. 3c), the stability of paratungstate B increases, offsetting the orthotungstate stability to higher pH. At this concentration of tungsten, a-metatungstate dominates up to pH ~4.5. At 4.5 = pH = 7.1, most tungsten is present as paratungstate B. At pH > 7.1, orthotungstate is the dominant species.

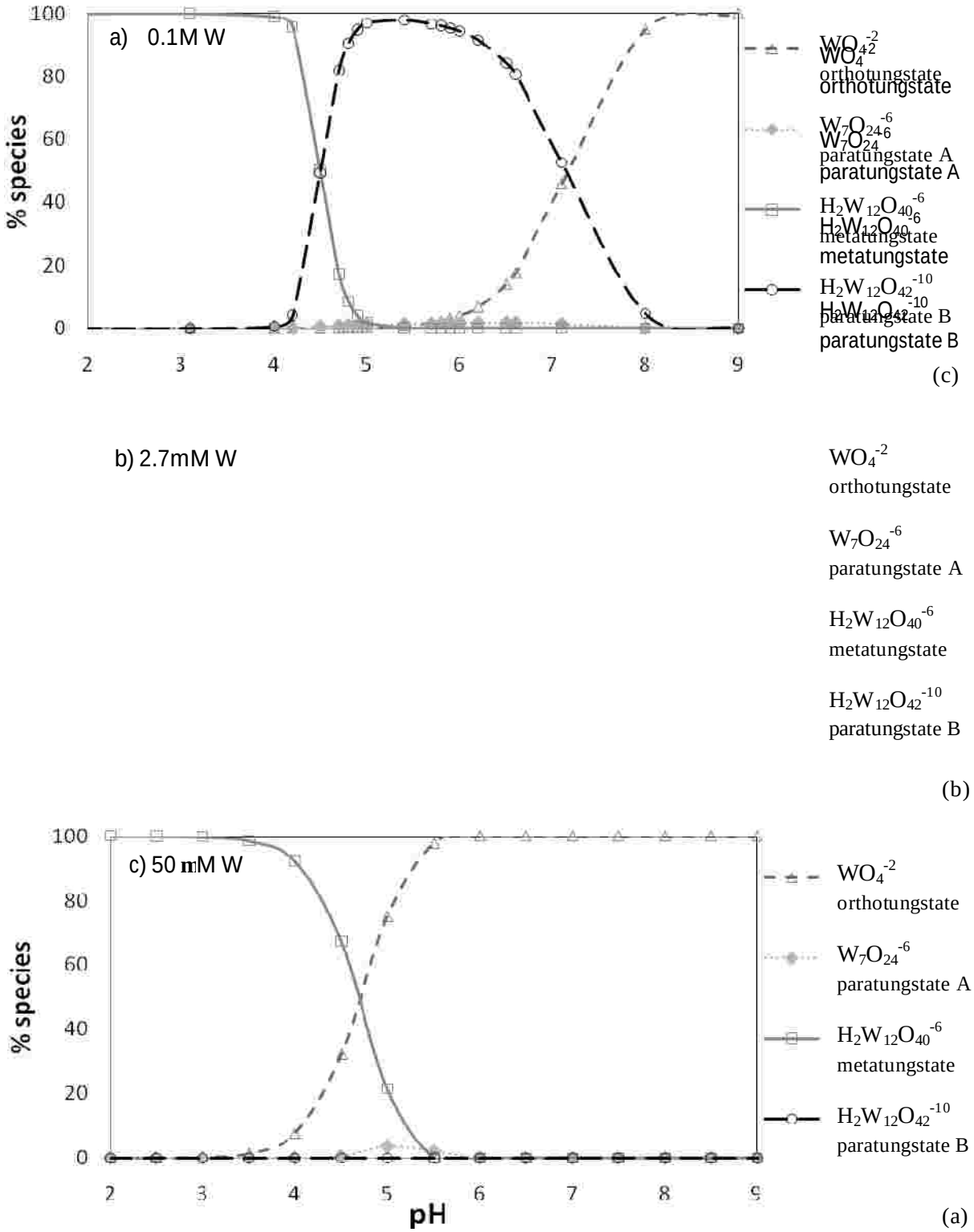

Figure 3. Calculated W(VI) speciation at a) 0.1 M, b) 2.7 mM and c) 50 μM W.

3.2. Batch Uptake Experiments

An adsorption isotherm of tungstate on goethite was developed at pH 4 for the range of initial tungsten concentrations of 50-1000 µM (Figure 4). This pH value was chosen because at pH 4 the surface charge of goethite is predominantly positive favoring anion adsorption. As expected, the amount of W sorbed at the surface of the goethite increases as the tungsten concentration in suspension increases.

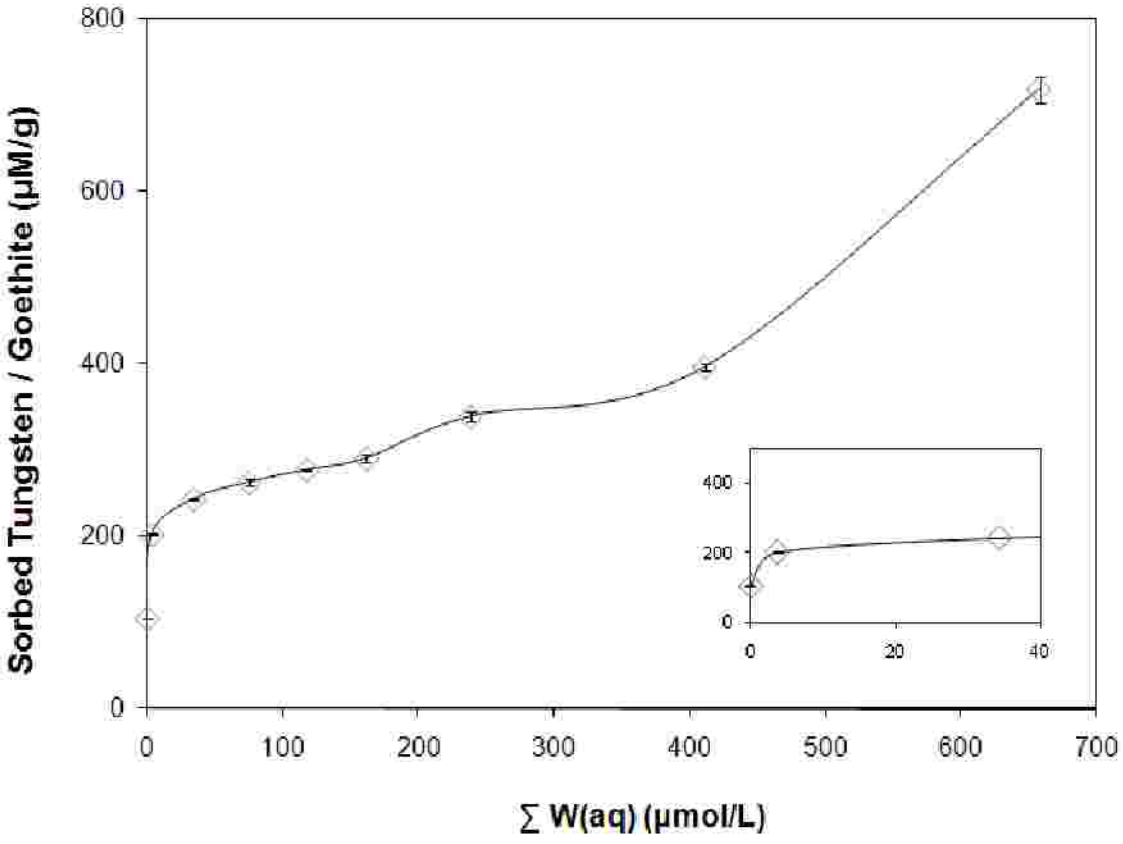

Figure 4. Adsorption isotherm of tungsten on goethite from a solution at pH 4.0, with 0.3 g/L Fe as goethite, and background electrolyte 0.01 M NaCl Error bars represent the standard error of the averaged repeated measurements.

The effect of pH on adsorption was investigated at an ial tungsten concentration of 50 µM by titrating separate goethite suspensions to pH values over the range 3-10 (Figure 5). The pH was re-measured after reaction because minor changes were observed in some suspensions after addition of W. The final pH value is represented in Figure 5. Characteristic anion adsorptive behavior is observed over a broad pH range with the greatest sorption occurring at acidic conditions. At pH = 5, approximately 100% sorption of tungsten occurs, with 50% sorption occurring at pH ~7.5. At pH greater than 8.5, less than 30% sorption is observed.

Figure 5. pH dependence of W sorption on goethite. Total W = 50 µM, 0.3 g/L Fe (as FeOOH), and background electrolyte is 0.01 M NaCl. Error bars represent the standard error of the averaged repeat measurements.

3.3. XANES Data

While the W L_{III}-edge EXAFS data provide information regarding the local environment of tungsten (including the number of nearest neighbors and their distances), the W L_I-edge XANES spectra are more sensitive to specific aspects of coordination such as oxidation state and whether the tungsten is tetrahedrally or octahedrally coordinated. XANES data for select model compounds, three solution samples and four sorption samples are shown in figure 6a. The intensity of the pre-edge feature (shown by the dotted line) is sensitive to the local coordination of tungsten (Kuzmin and Purans, 1993; Kuzmin and Purans, 2001; Yamazoe, 2008). The position of the pre-edge feature provides information regarding the electronic state of the species (Yamazoe, 2008). Note that the spectra for the four sorption data all look s lar; this will be addressed later.

Figure 6b shows the normalized absorption for the model compounds. It is confirmed from the position of the main edge (approximately 12.11-12.13 keV) that all of these compounds have the same oxidation state (6+). F 6c and 6d show W L_I-edge spectra of the pre-edge region for the model compounds. A prominent high intensity peak in the pre-edge region is indicative of tetrahedrally-coordinated tungsten. This is seen for scheelite ($CaWO_4$) and sodium tungstate dihydrate ($Na_2WO_4 \cdot H_2O$), which both have greater relative normalized absorption intensities (at ~0.75-0.9). The pre-edge region exhibits a lower intensity feature when tungsten is octahedrally coordinated (e.g. ferberite ($FeWO_4$), phosphotungstic acid ($H_3PO_4 \cdot 12WO_3 \cdot xH_2O$), tungsten trioxide ($WO_3$), and Ba_2NiWO_6). The intensity of the pre-edge region for the octahedrally coordinated compounds is sensitive to the degree of distortion. Ferberite, phosphotungstic acid and tungsten trioxide have distorted octahedra, so their pre-edge features have greater relative

normalized absorption intensities (~0.45-0.5) compared to Ba_2NiWO_6 (~0.3) , which is composed of perfect tungsten octahedra.

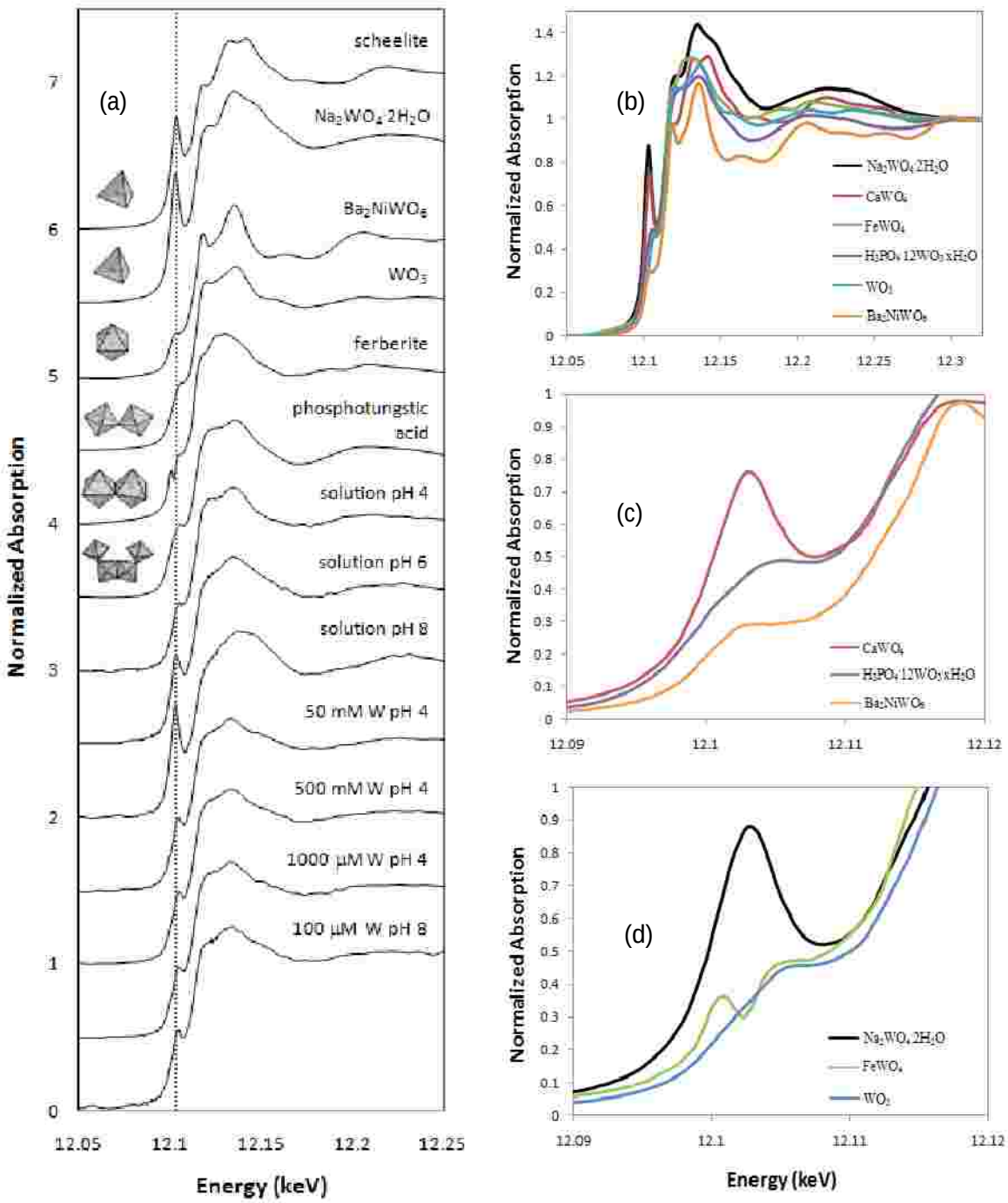

Figure 6a-d. Normalized W L_I-edge XANES spectra.

Figure 7 shows XANES spectra of three model compounds and three 2.7 mM tungstate solutions titrated to different pH values (4, 6 and 8). The intensity of the pre-edge feature from the pH 4 solution is lower than the pH 6 and 8 solutions and is similar in intensity to the feature from the $H_3PO_4 \cdot 12WO_3 \cdot xH_2O$ reference spectrum, indicating distorted octahedral coordination. The intensity of the pre-edge feature for the pH 8 solution is high, similar to the $Na_2WO_4 \cdot H_2O$ reference spectrum, indicating tetrahedral coordination. The relative normalized absorption intensity of the pre-edge feature for the pH 6 solution (~0.6) is intermediate between those of the pH 4 and 8 solutions, and it is unlike any of the reference compounds. This is thought to be the result of both tetrahedral and octahedral tungsten present in solution and is discussed later.

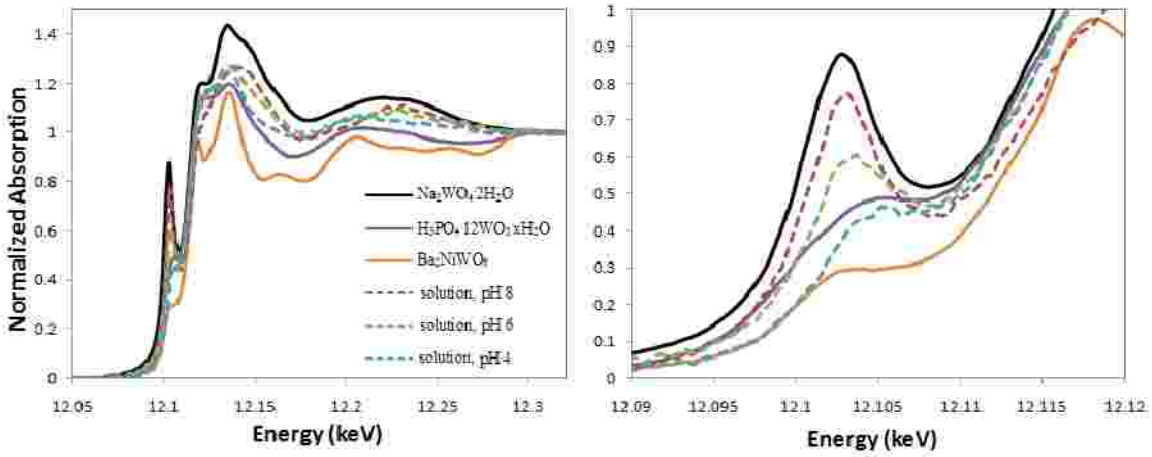

Figure 7. Normalized W L_I-edge XANES spectra for 2.7 mM W solutions at pH 4, 6 and 8 (dotted lines) as well as model compounds $Na_2WO_4 \cdot H_2O$, $H_3PO_4 \cdot 12WO_3 \cdot xH_2O$ and Ba_2NiWO_6 (solid lines) for comparison.

Figure 8 shows XANES spectra for three reference compounds and the 50µM W goethite sorption sample at pH 4. Only one sorption spectrum is shown because the data

for all of the sorption samples are similar. The intensity of the pre-edge feature for the sorption sample is similar to the intensity seen for $H_3PO_4 \cdot 12WO_3 \cdot xH_2O$, indicating distorted octahedral coordination.

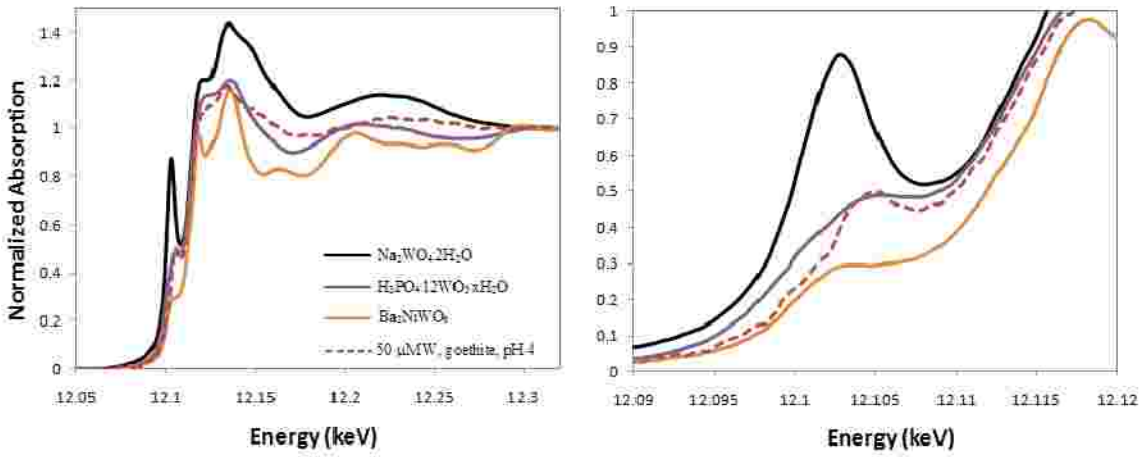

Figure 8. Normalized W L_I-edge XANES spectra for 50 µM W sorbed on goethite, pH 4 (dotted line) as well as model compounds $Na_2WO_4 \cdot H_2O$, $H_3PO_4 \cdot 12WO_3 \cdot xH_2O$ and Ba_2NiWO_6 (solid lines) for comparison.

3.4. EXAFS results for solution samples at pH 4, 6 and 8

The W L_{III}-edge EXAFS data of the 2.7 mM (500 ppm) W solution at pH 8 (Figure 9a) is dominated by a single beat, and the corresponding Fourier transform (Table 9b) shows a single peak. These data are best f ith a single 4-coordinated oxygen shell at 1.778 Å (Table 3) indicating that the species in solution is tetrahedral orthotungstate (WO_4^{-2}).

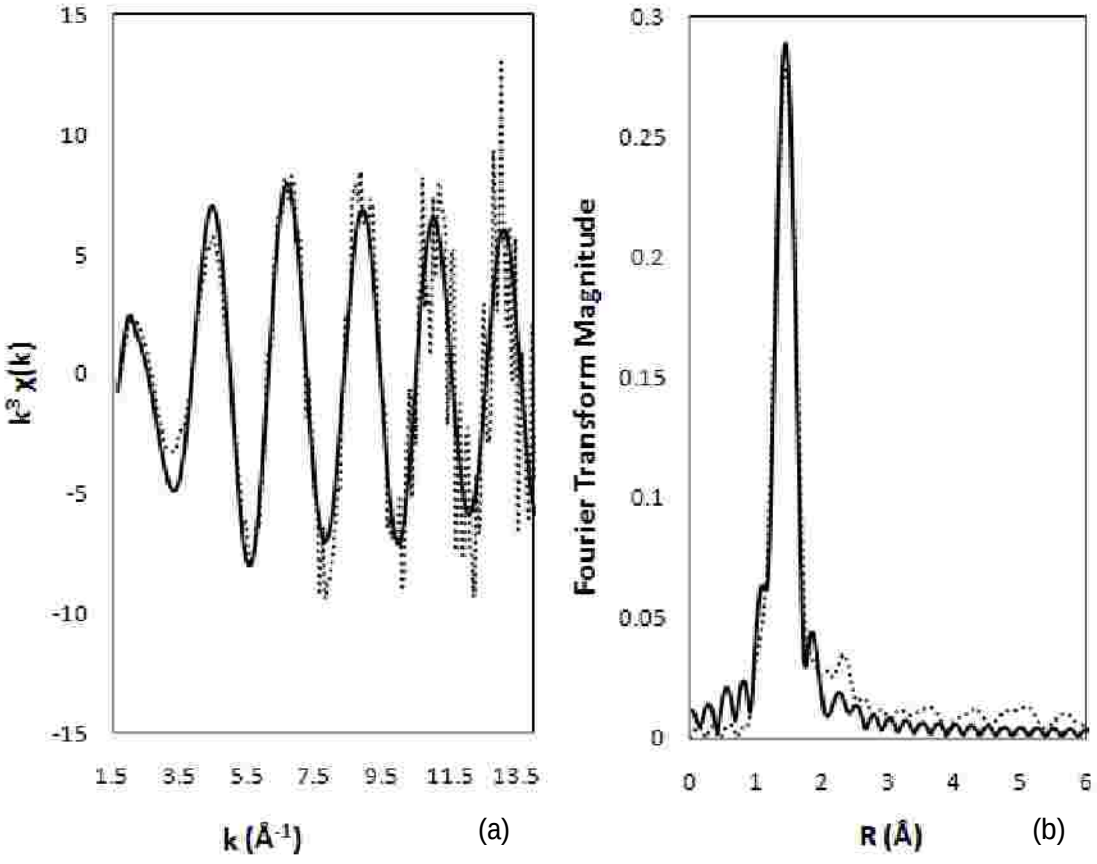

Figure 9. (a) k^3-weighted W L_{III}-edge EXAFS data of the 2.7 mM solution at pH 8, and (b) corresponding Fourier transforms. Data (dotted lines) and fit (solid lines).

Table 3. W LIII-edge EXAFS fitting results of 2.7 mM W solution at pH 8.
* denotes fixed

shell	CN	R (Å)	σ^2 (Å^2)	E_0 (eV)	S_0^2	Residual %
O	4.6	1.786	0.001	7.45	0.9*	11.95

The W L_{III}-edge EXAFS results for the 2.7 mM tungsten solutions at pH 4 and 6 are not as straightforward. As stated previously, tungstate forms polymeric species in acidic solutions, and the kinetics of polymerization are known to be sluggish. Similarities in local coordination among the polytungstates make it difficult to distinguish which species is (are) present by using EXAFS alone; this will be discussed later.

The EXAFS data and corresponding Fourier transform for the pH 4 solution are shown in Figure 10. The first shell of the Fourier transform is clearly split, and there is a substantial second shell peak at approximately 3.0-4.0 Å (not corrected for phase shift). Two strategies were used to fit these data (Table 4). One strategy used single scatter paths only to fit features at high R. This strategy fit the first shell with 2.2 oxygen atoms at 1.73 Å, 3.0 oxygen atoms at 1.89 Å and 1.0 oxygen atom at 2.25 Å, indicating distorted octahedral coordination. The second shell is fit with 2.0 tungsten atoms at 3.29 Å, 5.5 tungsten atoms at 3.58 Å and 4.9 tungsten atoms at 3.97 Å as well as 4.1 oxygen atoms at 3.24 Å, 8.4 oxygen atoms at 3.41 Å and 0.4 oxygen atoms at 3.97 Å. The second strategy used both single and multiple scatter paths to fit the features at high R. This strategy fit the first shell with 0.8 oxygen atoms at 1.70 Å, 4.2 oxygen atoms at 1.86

Å and 0.9 oxygen atoms at 2.24 Å, also indicating distorted octahedral coordination. In addition to multiple scatter and W-O contributions, these data are fit with 3.4 tungsten atoms at 3.29 Å and 0.8 tungsten atoms at 3.67 Å . Both fit strategies suggest the presence of a polytungstate and will be addressed in the discussion. It is important to note that for both fits the coordination numbers for second-shell oxygens are unrealistically high and will also be discussed later.

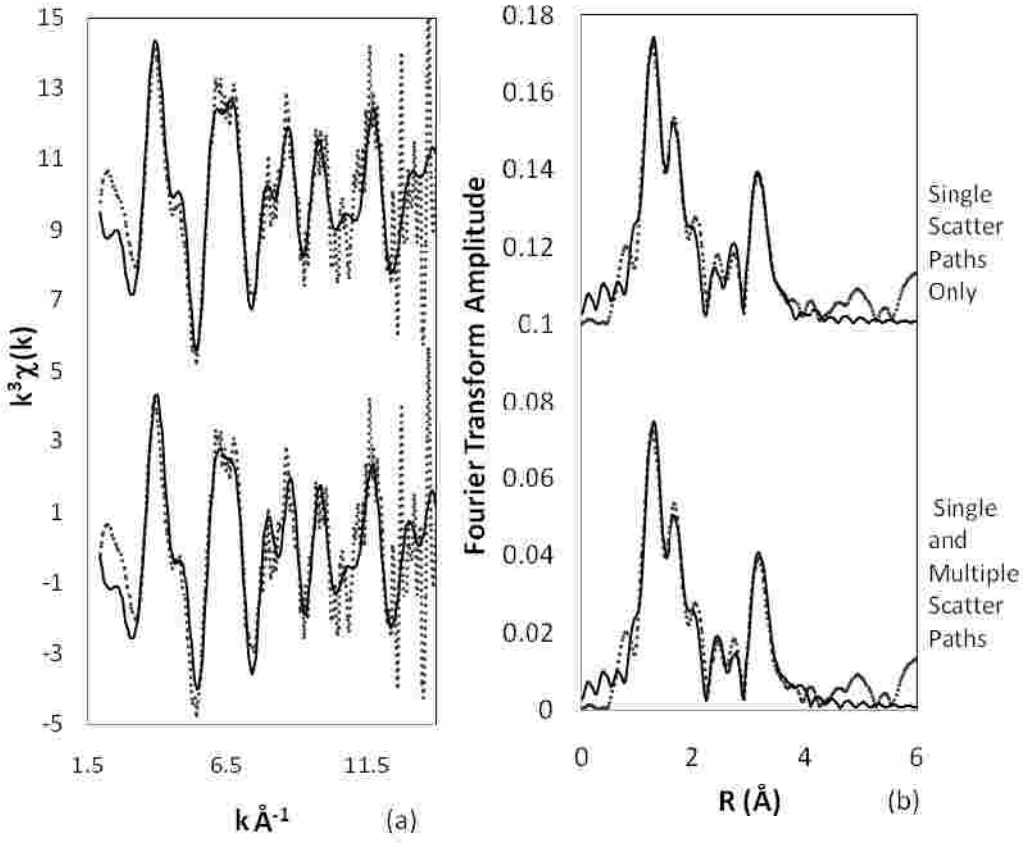

Figure 10. (a) k^3-weighted W L_{III}-edge EXAFS data of the 2.7 mM solution at pH 4, and (b) corresponding Fourier transforms in raw (dotted lines) and fitted data (solid lines).

Table 4. W L_{III}-edge EXAFS fitting results of 2.7mM W solution at pH 4 using (a) single scatter paths only, and (b) both single and W-O multiple scatter paths

(a) Single Scatter Paths Only						
shell	CN	R (Å)	σ^2 (Å^2)	E_0 (eV)	S_0^2	Residual %
O	2.2	1.73	0.0036	1.92	0.9*	18.29
O	2.9	1.89	0.0050			
O	1.0	2.25	0.0011			
W	2.0	3.29	0.0167			
O	4.1	3.24	0.0001			
W	5.5	3.31	0.0061			
O	8.4	3.41	0.0001			
W	4.9	3.58	0.0369			
O	0.4	3.97	0.0001			
(b) Single & Multiple Scatter Paths						
shell	CN	R (Å)	σ^2 (Å^2)	E_0 (eV)	S_0^2	Residual %
O	0.8	1.70	0.0004	1.92	0.9*	20.86
O	4.2	1.86	0.0089			
O	0.9	2.24	0.0001			
MS	12.0	3.16	0.0009			
MS	12.0	3.22	0.05			
O	5.3	3.27	0.0059			
W	3.4	3.29	0.0054			
O	4.8	3.43	0.0001			
W	0.8	3.67	0.0051			
* fixed						

The intensity of the pre-edge feature for the pH 6 solution in the W L_I-edge XANES is intermediate between the pH 4 and pH 8 solutions. Also, the speciation data indicate that orthotungstate and polytungstates are present in solution at pH 6. Even though our EXAFS data were collected on solutions that had not reached equilibrium, we considered the possibility that the species present in our pH 6 solution were similar to the polytungstates in our pH 4 solution and the tetrahedral tungsten present in pH 8 solution as suggested by XANES spectra and speciation calculations.. To explore this, we used

the k^3-weighted chi curves of pH 4 and 8 solutions as end members to perform a linear combination fit to determine speciation at pH 6. A linear combination fit using k^2-weighted chi curves of the pH 4 and 8 solutions as end members was done for comparison. The results were within 10 % of the k^3-weighted linear combination fit (Figure 11), which suggests that in the 2.7 mM W solution at pH 6, 38 % of the species in solution is orthotungstate while 62 % of the species in solution is whichever polytungstate(s) is/are present in the pH 4 solution. The dissimilarity apparent between the pH 4 and 8 end member spectra make linear combination fitting an effective analytical method, increasing our confidence in these results.

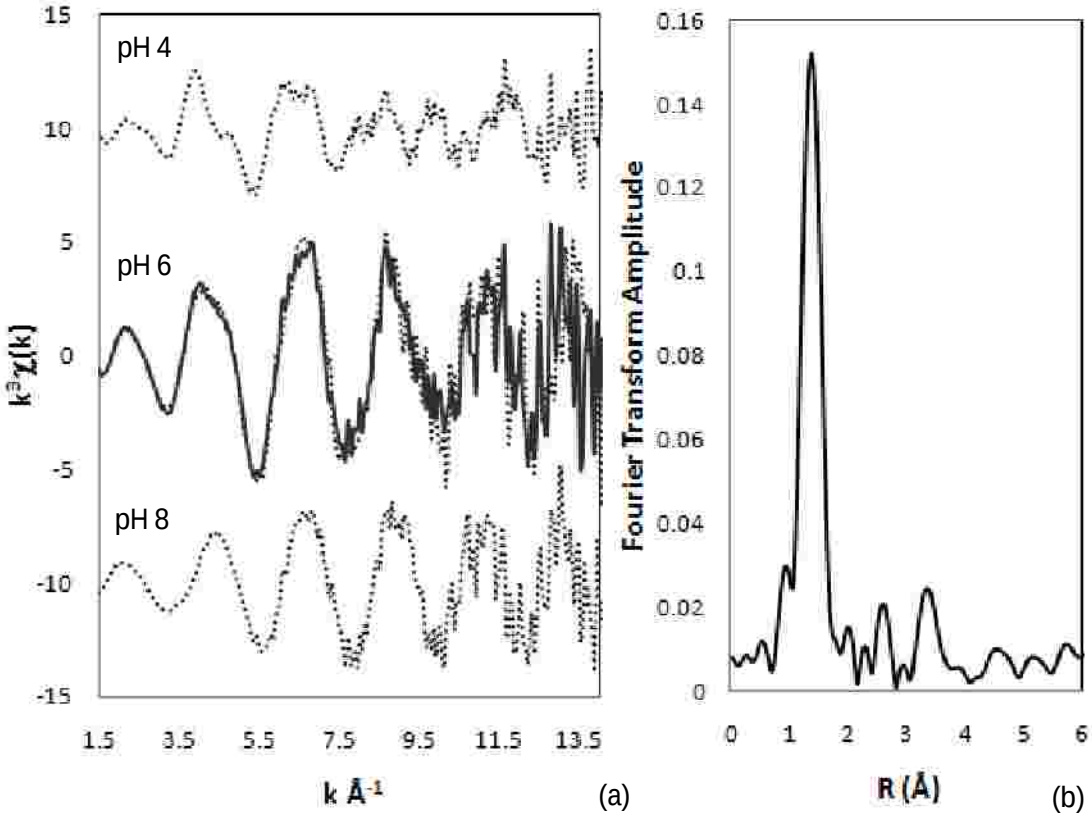

Figure 11. (a) W L_{III}-edge k^3-weighted EXAFS data of 2.7 mM W solution at pH 4, 6 and 8 (dotted lines) with k^3-weighted linear combination fit of the pH 6 solution (solid line) and (b) the Fourier transform of the EXAFS data for the solution at pH 6.

3.5. EXAFS results for model compounds

W L_{III}-edge EXAFS data of the model compounds are shown in Figure 12. In fitting certain known structures, coordination numbers were fixed. Two different approaches were used to fit model compounds. Na_2WO_4, scheelite, WO_3 and H_2WO_4 were all fit with every single scatter path calculated by FEFF6 according to the published structure. Multiple scatter paths were included in fits of H_2WO_4, Na_2WO_4 and WO_3 to improve quality. The second approach, used to fit ferberite and phosphotungstic acid, used a reduced number of paths, which were determined by trial and error to be the minimum number of paths necessary to get a good fit. Where multiple paths for the same backscatterer are present at similar distances, only one path was used, allowing for a correction of the coordination number. Due to the lar s used in certain fits, only first shell oxygens as well as second shell W and Fe contributions for each model compound are shown in Table 5. Sodium tungstate (Na_2WO_4) and scheelite ($CaWO_4$) both contain tungsten in perfect tetrahedral coordination with four oxygens at 1.79 Å and four tungstens at approximately 3.9 Å. Phosphotungstic acid ($H_3PO_4 \cdot 12WO_3 \cdot xH_2O$) has tungsten in distorted octahedra with two tungsten atoms at 3.39 Å (corresponding to edge-sharing) and two tungsten atoms at 3.72 Å (corresponding to corner sharing). Ferberite ($FeWO_4$) has tungsten in distorted edge-shared octahedral chains, with two tungsten atoms at 3.23 Å as well as four iron atoms at 3.45 Å and four at 3.62 Å. Tungsten trioxide (WO_3) was fit with 2.2 oxygen atoms at 1.76 Å, 1.8 oxygen atoms at 1.9 Å and 1.8 oxygen atoms at 2.15 Å as well as three tungsten atoms at 3.78 Å, which is consistent with the distorted corner-sharing octahedra present in the compound.

H_2WO_4 also has distorted corner-shared octahedra, and was fit with 0.9 oxygens at 1.71 Å, 1.8 oxygen atoms at 1.82 Å, 2.3 oxygen atoms at 1.92 Å and 1.6 oxygen atoms at 2.29 Å as well as 4 tungsten atoms at 3.76 Å.

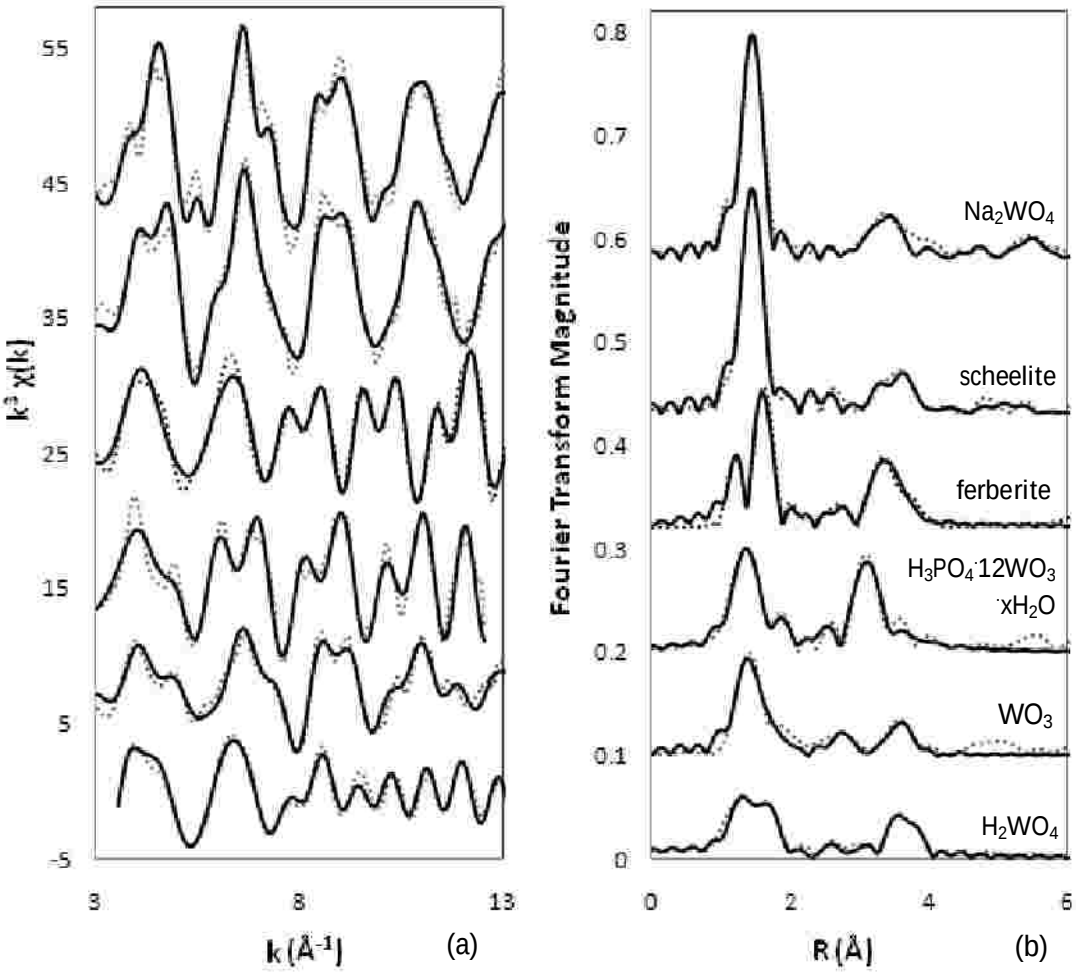

Figure 12. (a) W L_{III}-edge k^3-weighted EXAFS data of model compounds (H_2WO_4, WO_3, ferberite, scheelite, Na_2WO_4) and (b) the corresponding Fourier transforms (not corrected for phase shift). Data are shown as dotted lines and fits as solid lines

Table 5. W L_{III}-edge EXAFS fitting results of model compounds.

shell	CN	R (Å)	σ^2 (Å^2)	E_0 (eV)	S_0^2	Residual %
Na2WO4						
O	4*	1.79	0.0018	7.93	0.9*	17.6
W	4*	1.79	0.0122			
scheelite						
O	4*	1.79	0.0015	8.66	0.9*	16.9
W	4*	3.89	0.0145			
phosphotungstic acid						
O	1*	1.67	0.0007	2.97	0.9*	23.67
O	2*	1.91	0.0001			
O	2*	1.82	0.0034			
O	1*	2.31	0.0038			
W	2*	3.39	0.0028			
W	2*	3.72	0.0025			
ferberite						
O	2*	1.76	0.0009	3.37	0.9*	14.3
O	2*	1.88	0.001*			
O	2*	2.1	0.0048			
W	2*	3.23	0.0016			
Fe	4*	3.45	0.0056			
Fe	4*	3.62	0.0092			
WO_3						
O	2.2	1.76*	0.0023	4.75	0.9*	22.1
O	1.8	1.9*	0.1110			
O	1.8	2.15*	0.0032			
W	3*	3.78	0.0057			
H_2WO_4						
O	0.85	1.71	0.0005	6.82	0.9*	11.6
O	1.84	1.82	0.0026			
O	2.29	1.92	0.0038			
O	1.59	2.29	0.0106			
W	4*	3.76	0.0054			
* fixed						

3.6. EXAFS analysis of Sorption Samples

W L_{III}-edge EXAFS data and corresponding Fourier transforms of multiple sorption samples are shown in Figure 13 along with three model compounds for comparison. The sorption data are for samples prepared using different sorbents (goethite, ferrihydrite) over a range of pH (4-8) and tungsten concentration (25-1000 μM). Though the signal to noise ratio at high k varies for each sorption sample, the chi curves are clearly similar, showing a flattening of the curve at approximately 4 $Å^{-1}$ and a sharp peak at approximately 7 $Å^{-1}$. The Fourier transforms for the sorption samples show a single first-shell peak at approximately 1.37 Å and a prominent second-shell feature at approximately 3.12 Å (both shown with gray lines, not corrected for phase shift).

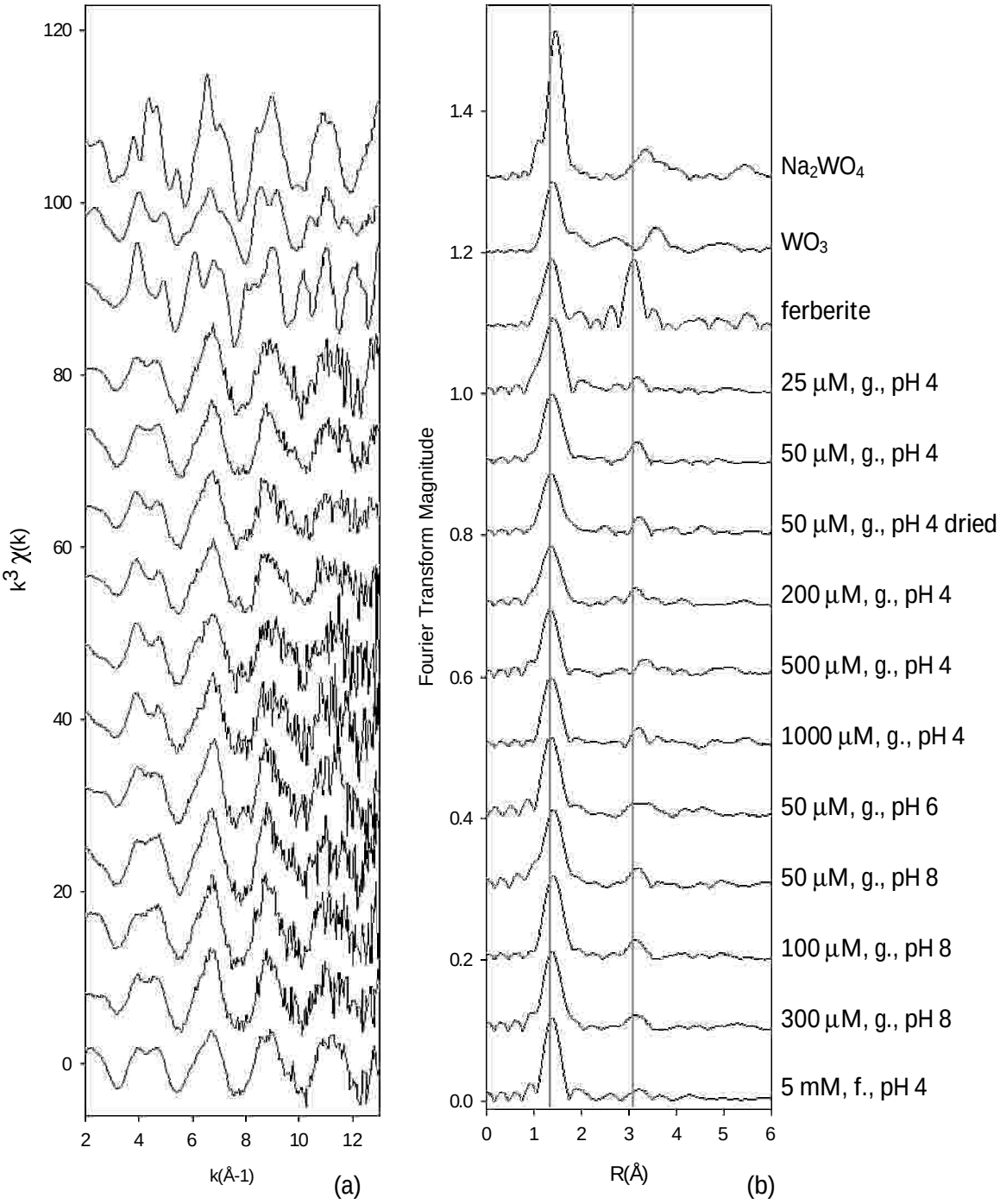

Figure 13. (a) k^3-weighted W L_{III}-edge EXAFS data for Na_2WO_4, WO_3, ferberite and tungsten sorption samples of various concentrations at pH 4, 6 and 8, and (b) corresponding Fourier transforms. g. (goethite is sorbent). f. (ferrihydrite is sorbent).

We observed that the FT of sorption samples shows two weak features at 2.0-2.5 Å (not corrected for phase shifts). In preliminary fitting we were not able to account for these features with backscattering from atoms at distances that could be explained by first or second shell coordination. Nor could these features be accounted for by multiple scattering. Therefore, we considered that they might arise due to inadequacies in background subtraction. W L_{III}-edge EXAFS data for one goethite sorption sample prepared at pH 4 with a concentration of 50 μM tungsten is shown in Figure 14, along with the corresponding transform. By varying the k-range used for Fourier transformation, we observed that these features varied in intensity. As the k-range is decreased so is the intensity of the two weak features (at 2.0-2.5 Å), while the two prominent features shown by the gray lines (at 1.37 and 3.12 Å, not corrected for phase shift) remain unchanged. Since the features at 2.0-2.5 Å are artifacts of background subtraction, they are not included in data fitting.

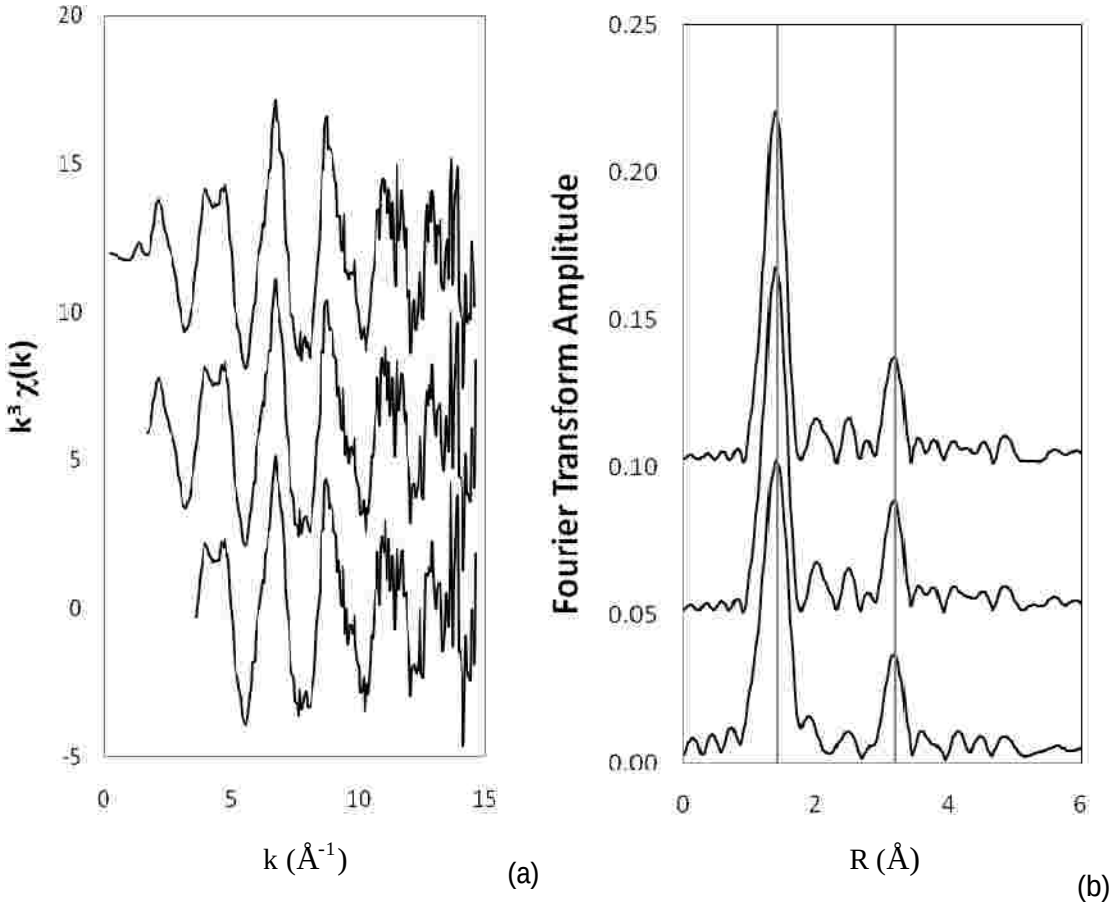

Figure 14. (a) k^3 –weighted W L_{III}-edge EXAFS data of 50 µM W sorbed at the surface of 0.5 g/L goethite at pH 4 with varied k ranges and (b) corresponding Fourier transforms.

The first shell of the 50 µM W on goethite spectrum at pH 4 is fit with 3.1 oxygen atoms at 1.76 Å and ~2.5 oxygen atoms at ~2.16 Å, which indicates distorted octahedral coordination (Figure 15). Two different strategies were used to fit the second shell (Table 6); both included a multiple scatter path with a fixed coordination number of 12 at ~3.15 Å. The first strategy used W-W paths to fit the feature at 3.12 Å with 1.2 tungsten atoms at 3.29 Å and 3.3 tungsten atoms at 3.74 Å. The second strategy used both W-W and W-Fe paths and fit the same feature with 2.0 tungsten atoms at 3.39 Å, 0.5 tungsten atoms at 3.74 Å and 1.5 iron atoms at 3.54 Å. The tungsten-tungsten coordination

numbers and distances (ranging from 3.2-3.8 Å) from both fits suggest the presence of polytungstate species sorbed at the surface as will be discussed later.

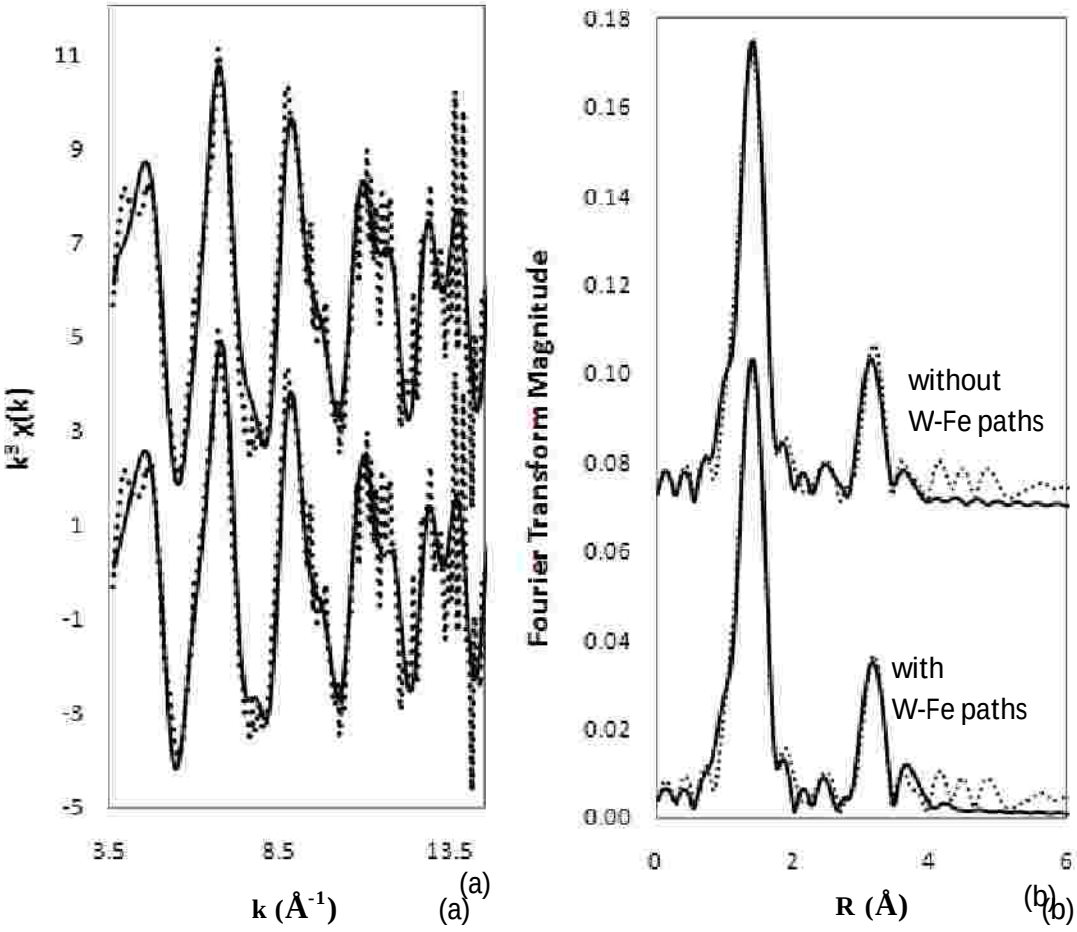

Figure 15. (a) fit of k^3-weighted W L_{III}-edge EXAFS data of the 50 µM W on 0.5 g/L goethite at pH 4 without W-Fe paths (above) and with W-Fe paths (below), and (b) corresponding Fourier transforms. (Raw data is dotted. Fit is Solid)

Table 6. W L_{III}-edge EXAFS fit results of 50 μM W sorbed on 0.5 g/L goethite at pH 4 using (a) without W-Fe paths and (b) with W-Fe paths.

(a)without W-Fe path						
shell	CN	R (Å)	σ^2 (Å^2)	E_0 (eV)	S_0^2	Residual %
O	3.1	1.76	0.004	3.05	0.9*	11.84
O	2.5	2.17	0.015			
MS	12*	3.11	0.0006			
W	1.2	3.29	0.0038			
W	3.3	3.74	0.0156			
(b)with W-Fe path						
shell	CN	R(Å)	σ^2(Å^2)	E_0 (eV)	S_0^2	Residual %
O	3.1	1.76	0.004	1.14	0.9*	11.25
O	2.4	2.16	0.0127			
MS	12*	3.18	0.0032			
W	2.0	3.39	0.0069			
Fe	1.5	3.54	0.0019			
W	0.5	3.74	0.0036			
* fixed						

3.7. Differential PDF data of Ferrihydrite Sorption Samples

The main features in the chi functions and FTs for the W-sorbed ferrihydrite sample are similar to those for the goethite sorption samples, except for minor differences in amplitude (Figure 16). Fitting also gives similar results, and it is difficult to determine if there is a W-Fe contribution, or if the second shell feature is due solely to tungsten. In an effort to provide further structural information, we examined differential pair distribution function (PDF) data collected on W-sorbed and W-free ferrihydrite samples. Synchrotron total X-ray scattering data for 2-line ferrihydrite and W-sorbed 2-line ferrihydrite were collected by Dr. Richard Harrington at 11-ID-B at the Advanced Photon Source, Argonne National Laboratory. The wavelength used was 0.2127 Å. The blank ferrihydrite data were subtracted from the W-sorbed sample, generating a new spectrum that, in principle, is attributable to scattering from the sorption complex (Figure 17). The advantage of this method is that structural information can be obtained over greater length scales than provided by EXAFS, and it is not limited to pairs involving tungsten only.

From this differential PDF spectrum (figure 17), multiple peaks are evident over length scales from 1.8 to 11.0 Å. The peak at 1.8 Å is readily attributable to the first-shell W-O distance. Higher-R peaks are not readily assigned, but the strong scattering power of tungsten makes it probable that the high R peaks involve a W component, and most likely a W-W pair. W-W distances in polytungstate species range from approximately 3.3 to 9.3 Å. Hence, we tentatively attribute the high R peaks in the differential PDF to W-W correlations.

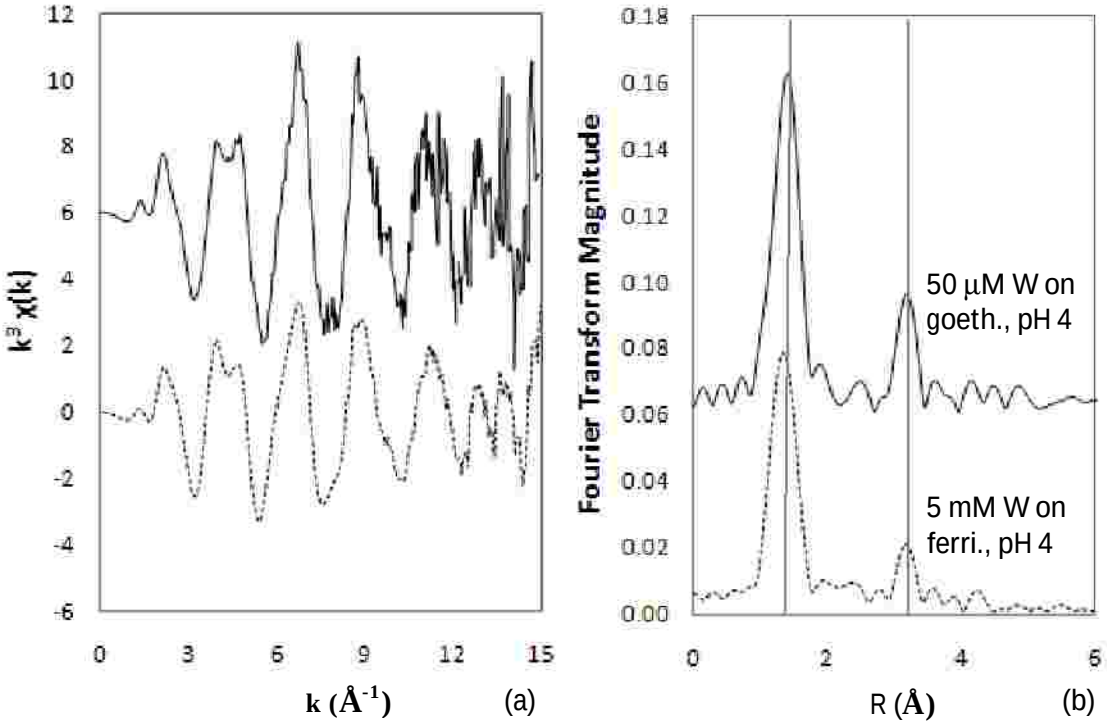

Figure 16. (a) k^3-weighted W L_{III}-edge EXAFS data of the 50 μM W on 0.477 g/L goethite at pH 4 (solid line) and 5 mM W on 0.5g/L ferrihydrite at pH 4 (dotted line), and (b) corresponding Fourier transforms.

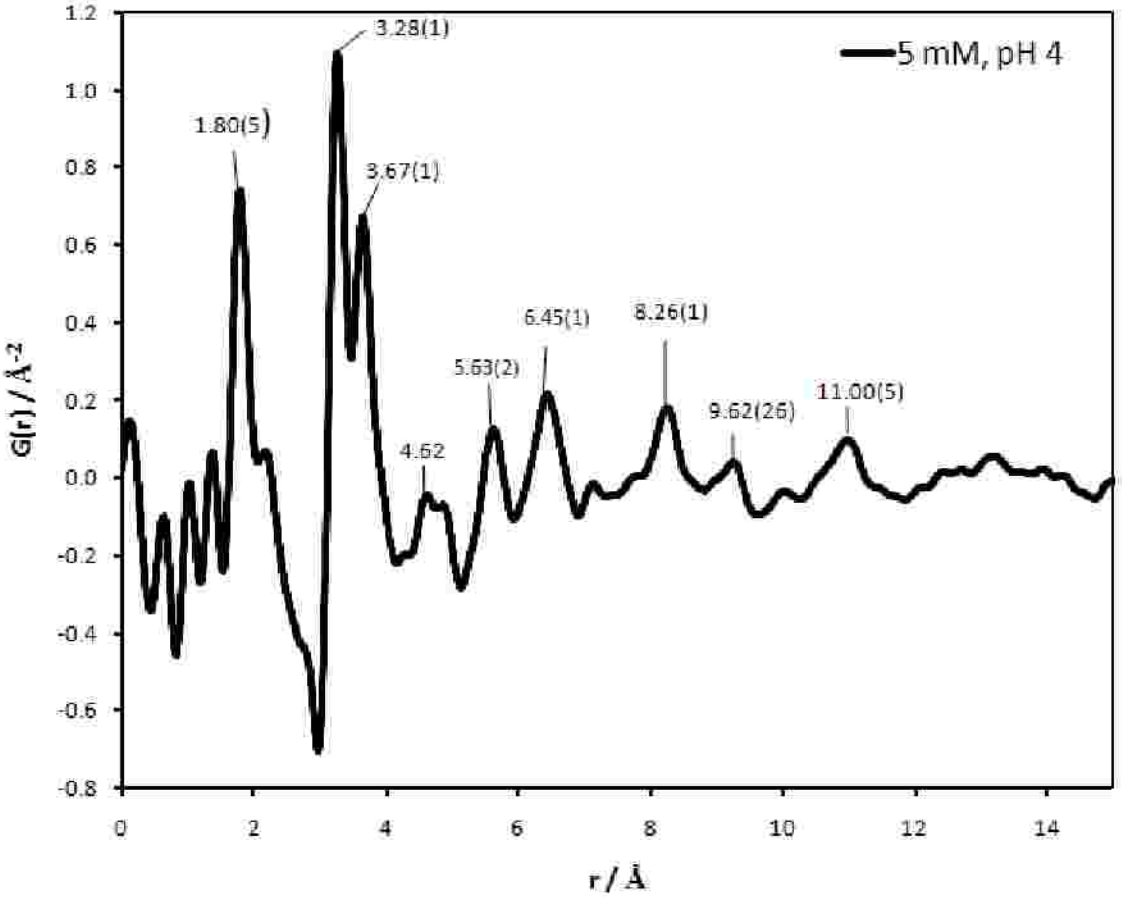

Figure 17. Differential PDF spectrum of 5 mM tungsten sorbed on 2-line ferrihydrite at pH 4.

4.Discussion

Batch uptake experiments show that W(VI) has a strong affinity for the goethite surface. The adsorption isotherm at low tungsten concentrations (50-300 μM) is similar to that published by other experimenters (Xu et al., 2 09), who concluded that W(VI) sorbs strongly and irreversibly at low pH. At higher ial concentrations (>300 μM W), the slope of the isotherm increases. A second increase in slope is seen as the initial concentration of W is increased from 600 to 1000 μM. The cause of these slope increases is unknown as we see no definitive evidence for precipitate formation. No other known experiments have examined tungstate sorption behavior at such high concentrations. As expected for an anion, tungstate sorbs preferentially at low pH. Tungsten's strong affinity for the goethite surface is evident from the ~20% that is observed to sorb at pH 10, which is above the point of zero charge for goethite (PZC~6.7 (Langmuir, 1997)).

The EXAFS data for the solution at pH 8 is fit with a single 4-coordinated oxygen shell at 1.78 Å, which is similar to the results from previous EXAFS work on tungstate solutions (Hoffmann et al., 2000). These results indicate that orthotungstate dominates in solution at pH 8, which is consistent with the aqueous speciation calculations for this tungsten concentration. It is also consistent with the XANES data, where the intensity of the pre-edge peak is similar to that seen for the tetrahedral reference compounds scheelite and sodium tungstate dihydrate.

It is difficult to identify particular polytungstate species or to rule out the presence of multiple polymeric species by EXAFS alone. The dif iculty arises from the fact that

polymeric tungstate species share common features of coordination, resulting in only subtle differences in local structure. EXAFS, which a ges over all tungsten atoms, can identify the main features of the local structure but is not sufficiently sensitive to distinguish among polymeric species. Nevertheless, we can use EXAFS to distinguish polytungstate species from orthothungstates because polymeric species have tungsten in distorted edge-sharing octahedral coordination, making W-W distances as short as 3.2 Å possible. The shortest possible W-W distance for corner sharing octahedra is approximately 3.6 Å.

The EXAFS data for the 2.7 mM W solution at pH 4 support the presence of polytungstates. From the fit of the first shell, it is evident that the tungsten is in distorted octahedral coordination because there are 6 (± 20 %) oxygen atoms at distances ranging from 1.7 to 2.2 Å. This is consistent with the XANES data of the pH 4 solution, which shows that the intensity of the pre-edge feature is similar to that seen for phosphotungstic acid, tungsten trioxide and ferberite, all of which contain distorted octahedrally-coordinated tungsten. From fits of the EXAFS for the 2.7 mM W solution at pH 4, the contribution of multiple scatter paths is difficult to determine, but there is an indisputable contribution from W at approximately 3.3 Å, indicating edge-sharing octahedra. This means at least one polytungstate is present in solution at pH 4. This is consistent with the speciation data, which shows polytungstate species dominant in solution at pH 4 regardless of tungsten concentration. Previous authors have found that second-shell tungsten as well as multiple scatter paths are important when fitting W L_{III}-edge EXAFS data of tungstate solutions and WO_3 (Hoffmann et al., 2000; Kuzmin, 1993), but even with MS paths included in our fit, coordination numbers were unreasonably high for

second-shell oxygens. These unrealistic coordination numbers may be due to additional complex multiple scatter contributions, multiple polytungstates present in solution or poor signal to noise.

EXAFS fitting of the pH 6 solution using a single model was not attempted because multiple species are thought to be present. This notion is supported by the XANES data, which show a pre-edge feature with an intensity that is intermediate between both the tetrahedral and octahedral model compounds and the pH 8 and 4 solutions. A linear combination fit of the pH 6 solution data using the pH 4 and 8 data as end-members suggests that orthotungstate represents 38% of the solution species and polytungstate(s) represents 62%. The speciation data do show multiple species (orthotungstate, paratungstate A and paratungstate B) to be present in a 2.7 mM W solution at pH 6, but the percentages differ from the LCF by approximately 10%. This is likely explained by error associated with the linear combination fit, which is estimated to be 5–10 %.

As described in the results section, both the W L_I-edge XANES spectra and the Fourier transformed k^3-weighted W L_{III}-edge EXAFS data for all of the goethite sorption samples are strikingly similar regardless of pH or tungsten concentration. Even the EXAFS spectrum for the ferrihydrite sample shows similar features. The first shell feature in the EXAFS spectrum of the goethite sample is fit with approximately 3 oxygens at 1.76 Å and approximately 2.5 oxygens at 2.17 Å, indicating distorted octahedral coordination. This is consistent with the XANES data. The second prominent feature at 3.0-3.8 Å in the Fourier transform is fit with tungsten atoms at 3.29-3.39 Å and 3.74 Å. Iron may also contribute, though it is difficult (maybe impossible) to discern this

from the data. The tungsten-tungsten distances indicate edge and corner sharing octahedra, which means a polytungstate is the most likely sorbed species. The notion of a sorbed polytungstate is supported by the differential PDF data which show peaks associated with the sorption products at 8-11 Å, which are reasonable W-W distances for polytungstate species. Also, polytungstate sorption products could explain why all of the XAS data look similar regardless of the dominant aqueo pecies, sorbent, pH or tungsten concentration.

Previous studies have used the charge distribution multi-site complexation model (CD-MUSIC) combined with experimental results to predict that the dominant tungstate complex bound to the goethite (110) surface at low pH is a diprotonated monodentate monomeric complex (Xu et al., 2006; Xu et al. 2009). Our direct spectroscopic results, however, do not support the presence of a mononuclear (orthotungstate) complex. Instead, we find that a polymeric tungstate(s) exists as the surface complex. Xu et al. reported that the monolayer capacity of tungstate at low pH is double that of phosphate; it is hypothesized that this may reflect multiple uptake mechanisms (adsorption, polymerization and precipitation) (Xu et al, 2009). Based on the results from this study, a re-evaluation of current tungstate sorption models may be useful in an assessment of tungsten's environmental behavior.

5. Conclusions and Implications

In this study, we have investigated the role of tungstate speciation on adsorption onto the goethite and ferrihydrite surfaces over a range of pH and concentration conditions. Tungstate has been shown to adsorb as a polymeric complex, even when orthotungstate is the dominant solution species. The surface seems to favor the formation of polymeric species, but the reasons for this require further study. The polymeric nature of the sorption complex is inferred from W-W distances at 3.29-3.39 and 3.74 Å typical of the edge and corner sharing octahedra, respectively, found in polytungstates.

The contribution from iron in the W L_{III}-edge EXAFS and differential PDF data requires further investigation. The strong scattering power of tungsten makes W-W contributions in the differential PDF more likely than W-Fe, though more exploration is necessary. Similar studies using sorbents other than iron oxides (e.g., Al-oxides) could help to resolve the extent of contribution from iron scattering in both the EXAFS and differential PDF data. Different sorbents could also help clarify the role of the iron oxide mineral surface in polymerization of tungstate sorption complexes.

Recent findings, which suggest that polytungstates are significantly more toxic than monotungstates (Strigul et al. a, in press; Strigul et al. b, in press), make polymerization at iron oxide mineral surfaces over a w a possible cause for concern. Additional research regarding the effect of speciation on tungsten toxicity and mobility are necessary for a more complete evaluation of the environmental fate of this unregulated metal.

References

ATSDR, 2005. Toxicological Profile for Tungsten. U.S. Department of Health and Human Services-Agency for Toxic Substances and Disease Registry.

Bednar, A. J., Jones, W. T., Boyd, R. E., Ringelberg, D. B., and Larson, S. L., 2008. Geochemical parameters influencing tungsten mobility in soils. *Journal of Environmental Quality* **37**, 229-233.

Burtseva, K. G., Chernaia, T. S., and Sirota, M. I., 1978. Determination of crystal-structure and molecular-structure of sodium paratungstate. *Doklady Akademii Nauk Sssr* **243**, 104-107.

Clausen, J.L. and Korte, N., 2009. Environmental fate of tungsten from military use. *Science and the Total Environment* **407**, 2887-2893.

Cruywagen, J. J. and Vandermerwe, I. F. J., 1987. Tungsten(VI) equilibria - A potentiometric and calorimetric investigation. *Journal of the Chemical Society-Dalton Transactions* **7** 1701-1705.

Davis, J. A. and Kent, D. B., 1990. Surface complexation modeling in aqueous geochemistry. *Reviews in Mineralogy* **23**, 177-260.

Dermatas, D., Braida, W., Christodoulatos, C., Strigul, N., Panikov, N., Los, M., and Larson, S., 2004. Solubility, sorption, and soil respiration effects of tungsten and tungsten alloys. *Environmental Forensics* **5**, 5-13.

Evans, H. T. and Rollins, O. W., 1976. Sodium paradodecatungstate 20-hydrate. *Acta Crystallographica Section B-Structural Science* **32**, 1565-1567.

Gustafsson, J. P., 2003. Modelling molybdate and tungstate adsorption to ferrihydrite. *Chemical Geology* **200**, 105-115.

Hastings, J. J. and Howarth, O. W., 1992. A W-183, H-1 and O-17 Nuclear-Magnetic-Resonance study of aqueous isopolytungstates. *Journal of the Chemical Society-Dalton Transactions* **2**, 209-215.

Hoffmann, M. M., Darab, J. G., Heald, S. M., Yonker, C. R., and Fulton, J. L., 2000. New experimental developments for in situ XAFS studies of chemical reactions under hydrothermal conditions. *Chemical Geology* **167**, 89-103.

Johnson, J. L., Cohen, H. J., and Rajagopa.Kv, 1974. Molecular-basis of biological function of molybdenum - molybdenum-free sulfite oxidase from livers of tungsten-treated rats. *Journal of Biological Chemistry* **249**, 5046-5055.

Johnson, J. L. and Rajagopalan, K. W., 1976. Electron paramagnetic resonance of the tungsten derivative of rat liver sulfite oxidase. *Journal of Biological Chemistry* **251**, 5505-5511.

Keggin, J. F., 1934. The Structure and Formula of 12-Phosphotungstic Acid. *Proceedings of the Royal Society of London. Series A, Containing Papers of a Mathematical and Physical Character* **144**, 75-100.

Kepert, D. L., 1962. Isopolytungstates. In: Cotton, F. A. (Ed.), *Progress in Inorganic Chemistry*. John Wiley & Sons, Inc., New York.

Koutsospyros, A., Braida, W., Christodoulatos, C., Dermatas, D., and Strigul, N., 2006. A review of tungsten: From environmental obscurity to scrutiny. Elsevier Science Bv.

Kuzmin, A. and Purans, J., 1993. The Influence of the focusing effect on the x-ray-absorption fine-structure above all the tungsten-L edges in nonstoichiometric tungsten oxides. *Journal of Physics-Condensed Matter* **5**, 9423-9430.

Kuzmin, A. and Purans, J., 2001. Local atomic and electronic structure of tungsten ions in AWO(4) crystals of scheelite and wolframite types. *Radiation Measurements* **33**, 583-586

Langmuir, D., 1997. *Aqueous Environmental Geochemistry*. Prentice Hall, Upper Saddle River, New Jersey.

Newville, M., 2001. IFEFFIT: Interactive EXAFS analysis and FEFF fitting. *Journal of Synchrotron Radiation* **8**, 322-324.

Pardus, M. J., Lemus-Olalde, R., and Hepler, D. R., 2009. Tungsten human toxicity: a compendium of research on metallic tungsten and tungsten compounds. *Land Contamination & Reclamation* **17**, pp. 217-222.

Parkhurst, D. L. and Appelo, C. A. J., 1999. User's Guide to PHREEQC (Version 2) -- A computer program for speciation, batch-reaction, one-dimensional transport, and inverse geochemical calculations. U.S. Geological Survey Water Investigations Report 99-4259, Denver, Colorado.

Petkewich, R., 2009. Unease over tungsten. *Chemical & Engineering News* **87**, 63-65.

Pope, M. T., 1983. Heteropoly and Isopoly Oxometallates. Springer-Verlag, Berlin.

Reeder, R. J., Schoonen, M. A. A., and Lanzirotti, A., 006. Metal speciation and its role in bioaccessibility and bioavailability. *Reviews in Mineralogy & Geochemistry: Medical Mineralogy and Geochemistry* **64**, 59-113.

Ressler, T., 1997. WinXAS: A new software package not only for the analysis of energy-dispersive XAS data. *J. Phys. IV* **7**, 269- 270.

Schwertmann, U. and Cornell, R. M., *Iron Oxides in the Laboratory, Preparation and Characterization*. VCH Publishers, New York.

Seiler, R. L., Stollenwerk, K. G., and Garbarino, J. R., 2005. Factors controlling tungsten concentrations in ground water, Carson Desert, Nevada. *Applied Geochemistry* **20**, 423-441.

Smith, B. J. and Patrick, V. A., 2000. Quantitative determination of sodium metatungstate speciation by W-183 NMR spectroscopy. *Australian Journal of Chemistry* **53**, 965-970.

Strigul, N., Galdun, C., Vaccari, L., Ryan, T., Braida, W., and Christodoulatos, C., in press, a. Influence of Speciation on Tungsten Toxicity.

Strigul, N., Koutsospyros, A., and Christodoulatos, C., in press, b. Tungsten speciation and toxicity: acute toxicity of mono- and poly- tungstates to fish. *Ecotoxicology and Environmental Safety*.

Strigul, N. S., Koutsospyros, A., and Christodoulatos, C., 2009. Tungsten in the former Soviet Union: review of environmental regulations and related research. *Land Contamination and Reclamation* **17**, 189-216.

van Put, J. W., 1995. Crystallisation and processing of ammonium paratungstate. *International Journal of Refractory Metals and Hard Ma rials* **13**, 61-76.

Xu, N., Christodoulatos, C., and Braida, W., 2006. Modeling the competitive effect of phosphate, sulfate, silicate, and tungstate anions on the adsorptio date onto goethite. *Chemosphere* **64**, 1325-1333.

Xu, N., Christodoulatos, C., Koutsospyros, A., and Braida, W., 2009. Competitive sorption of tungstate, molybdate and phosphate mixtures onto goethite. *Land Contamination & Reclamation* **17**, 45-57.

Yamazoe, S., Hitomi, Y., Shishido, T., and Tanaka, T., 2008. XAFS study of tungsten L-1- and L-3-edges: Structural analysis of WO_3 species loaded on TiO_2 as a catalyst for photo-oxidation of NH_3. *Journal of Physical Chemistry C* **112**, 6869-6879.

Zabinsky, S. I., Rehr, J. J., Ankudinov, A., Albers, R. C., and Eller, M. J., 1995. Multiple-scattering calculations of X-ray absorption spectra. *Phys. Rev. B* **52**, 2995-3009.